



EUROPEAN  
COMMISSION

Community research



## DOPAS Work Package 5

### Deliverable D5.7: Models and modelling summary report for EPSP

Grant Agreement number:	323273
Authors:	Markéta Dvořáková, Dmitry Lukin, Dagmar Trpkošová (SÚRAO and ÚJV Řež, a.s.)
Date of preparation:	February 2016
Version status:	1
Draft update status	1

Start date of the project: September 2012

Duration: 48 months

Project co-funded by the European Commission under the Euratom Research and Training Programme on Nuclear Energy within the 7 <sup>th</sup> Framework Programme (2007-2013)		
Dissemination level		
PU	Public	X
RE	Restricted to a group specified by the partners of the DOPAS project	
CO	Confidential, only for DOPAS partners	



Scope	Deliverable n°D5.7 (WP5)	Version:	1.0
Type/No.	Report	Total pages	2+65
		Appendixes	
Title	Deliverable n°5.7 Deliverable D5.7: Models and modelling summary report for EPSP	Articles:	

**ABSTRACT:**

This report provides an outline of the models constructed for, and a modelling summary report concerning the Experimental Pressure and Sealing Plug (EPSP) experiment.

**RESPONSIBLE:**

SURAO, Markéta Dohnálková

**REVIEW/OTHER COMMENTS:**

The document is reviewed according to the SURAO procedure

**APPROVED FOR SUBMISSION:**

Johanna Hansen, 31.8.2016



## Executive Summary

This report provides an outline of the models constructed for, and a modelling summary report concerning the Experimental Pressure and Sealing Plug (EPSP) experiment. The EPSP experiment is not intended to test a specific plug or seal; rather it has been constructed at a similar scale to a real disposal tunnel plug and will contribute specifically to the development of the reference design for such structures. The objective of the EPSP experiment is to test the materials and technology to be employed for implementation purposes, not to test the design or performance of reference disposal tunnel plugs. At this early stage in the Czech geological disposal programme, with more than 50 years to go before operation is scheduled to commence, it is considered more important to build knowledge and experience rather than to refine designs for implementation at an, as yet, unidentified site for which, clearly, it is not possible to detail specific mechanical, hydrogeological and chemical characteristics.

The main features, events and processes related to the proposed plug and sealing system have already been identified. Assessment has been divided into short-term assessment, which covers the operational period, and long-term assessment which takes into account the post-operational period. The main functional component with regard to the short-term period will consist of the concrete walls which it is intended will prevent the seepage of water from the disposal drifts. As far as the long-term period is concerned, the main component will consist of a compacted, saturated bentonite layer the function of which will be to seal any preferential paths which might be formed and to prevent the migration of radionuclides following the eventual failure of the canisters containing spent fuel assemblies. Modelling focuses primarily on the analysis of the THM properties of the various EPSP components.



## List of Acronyms

AECL:	Atomic Energy of Canada Limited.
ASN:	Autorité de Sûreté Nucléaire.
BAT:	Best available technique.
BMU:	Bundesministerium für Umwelt, Naturschutz und Reaktorsicherheit.
BSK-3:	BrennstabKokille-3.
CIGEO:	Centre Industriel de Stockage Géologique.
DBE:	Deutsche Gesellschaft zum Bau und Betrieb von Endlagern für Abfallstoffe mbH.
DOMPLU:	Dome Plug.
DOPAS:	Full-scale Demonstration of Plugs and Seals.
EBS:	Engineered barrier system.
EC:	European Commission.
EDZ:	Excavation damaged zone.
ELSA:	Entwicklung von Schachtverschlusskonzepten (development of shaft closure concepts)
EPSP:	Experimental Pressure and Sealing Plug.
ESDRED:	Engineering Studies and Demonstration of Repository Designs.
FEBEX:	Full-scale Engineered Barriers Experiment.
FSS:	Full-scale Seal.
GDF:	Geological disposal facility.
HADES:	High-activity Disposal Experimental Site.
HCB:	Highly-compacted bentonite.
HLW:	High-level waste.
HM:	Hydro mechanic
HRL:	Hard rock laboratory.
IAEA:	International Atomic Energy Agency.
ILW:	Intermediate-level waste.
IRF:	Instant release fraction
IRSN:	Institut de Recherche sur la Sûreté Nucléaire.
KBS-3:	KärnbränsleSäkerhet-3.
LLW:	Low-level waste.
MO <sub>x</sub> :	Mixed oxide



POPLU:	Posiva Plug.
R&D:	Research and development.
RCF:	Rock characterisation facility.
RESEAL:	A large scale <i>in situ</i> demonstration test for repository sealing in an argillaceous host rock.
RH	Relative humidity
RMS:	Requirements management system.
SCC:	Self-compacting concrete.
SF:	Spent fuel
TSX:	Tunnel sealing experiment.
UO <sub>2</sub> :	Uranium dioxide
URCF:	Underground rock characterisation facility.
URF:	Underground research facility.
URL:	Underground research laboratory.
VOP:	Vaatimuksia Ohjaava Päätös (Decisions Guiding Requirements).
VSG:	Vorläufige Sicherheitsanalyse Gorleben (Preliminary Safety Analysis for Gorleben).
WMO:	Waste management organisation.
WP:	Work package.



## List of DOPAS Project Partners

A list of the partners involved in the DOPAS Project is provided below. Each partner will be referred to in the remainder of this report as indicated:

ANDRA:	L'Agence nationale pour la gestion des déchets radioactifs.
B+ Tech:	B+ Tech Oy.
CTU:	Czech Technical University.
DBE TEC:	DBE TECHNOLOGY GmbH.
Galson Sciences:	Galson Sciences Limited.
GRS:	Gesellschaft für Anlagen- und Reaktorsicherheit.
Nagra:	Die Nationale Genossenschaft für die Lagerung Radioaktiver Abfälle.
NDA:	Nuclear Decommissioning Authority.
NRG:	Nuclear Research and Consultancy Group.
Posiva:	Posiva Oy.
SÚRAO:	Správa úložišť radioaktivních odpadů (The Czech Radioactive Waste Repository Authority).
SKB:	Svensk Kärnbränslehantering AB.
UJV:	ÚJV Řež, a.s.
VTT:	Teknologian Tutkimuskeskus VTT Oy.



## Table of Contents

Executive Summary .....	3
1. Background.....	8
2. Description of the laboratory work.....	8
3. Numerical modelling.....	15
3.1 Computer software employed .....	15
3.2 Conceptual model.....	16
4. Calibration of the numerical model .....	20
4.1 Numerical model of the PHM using bentonite powder.....	20
4.2 Numerical model of a PHM using bentonite pellets .....	26
5. Testing the influence of the sealing property of bentonite with respect to deep geological repository safety.....	33
5.1 Conceptual model.....	35
5.2 Parametric model settings.....	36
5.3 Degradation of the SF container.....	38
5.4 Bentonite damping and sealing layer .....	39
5.5 Simulation of an erosion channel .....	42
5.6 Geosphere .....	42
5.7 Biosphere .....	45
6. Results and discussion.....	51
7. Modelling of the EPSP experiment.....	60
7.1 Experiment description.....	60
7.2 Methodology and model.....	61
7.3 Geometry .....	62
7.4 Material parameters .....	62
7.5 Time intervals.....	63
7.6 Modelling Results.....	64
8. Conclusions .....	66
9. Literature .....	67



## 1. Background

The Czech Republic's deep geological repository (DGR) will be designed so as to ensure safety for a period of thousands of years. The Czech geological disposal programme for spent fuel and HLW is currently in the generic phase with no specific site having yet been selected. It is planned that construction work will commence in 2050 and operation in 2065.

As far as the Czech Republic is concerned solely crystalline rock formations can be considered for the construction of a deep geological repository. The Czech DGR concept states that nuclear waste will be encased in steel-based canisters placed in vertical or horizontal boreholes at a depth of ~ 500m below the surface. The space between the canisters and the host crystalline rock will be filled with compacted bentonite which will form the final engineered barrier. The waste packages will be emplaced in the disposal tunnels in the form of supercontainers. This concept formed the basis for generic safety assessment studies conducted in 2011. The steel-based canisters considered in the Czech concept as opposed to the copper-based canisters considered in the Swedish and Finnish concepts were selected based on the Czech Republic having greater industrial experience with the production of steel-based canisters, suggesting that there will be a substantially lower probability of the occurrence of initial defects in the canisters caused by human error during the manufacturing process, and due to the expected lower price of steel canisters compared to that of copper canisters. The conceptual design (rather than the manufacturing details) of plug and sealing systems was considered with reference to the Swedish KBS-3V and KBS-3H concepts. Although KBS-3H is now generally regarded as the reference concept, both the KBS-3H and KBS-3V designs will continue to be developed in parallel.

The first assessment concerning the disposal of spent fuel and HLW in the Czech Republic considered a generic reference concept based on KBS-3V (SÚRAO, 1999). The main aim of this PA was to summarise performance assessment requirements based on an analysis of Czech legislation and IAEA recommendations. However, subsequent performance studies focussed on a horizontal variant of the concept known as KBS-3H (SÚRAO, 2011). Plug and sealing systems were not considered in these preliminary safety assessments.

The 7<sup>th</sup> Framework Programme DOPAS project initiated a proposal for the design of plugs and seals that can be used for sealing disposal drifts and backfilled tunnels in the planned repository.

The design basis of the EPSP plug is based on experience gained as the result of the sealing of an underground gas storage facility located near the town of Příbram in the Czech Republic. The plugs used in the facility were constructed using steel fibre-reinforced sprayed concrete (SFRC). Trial plugs were employed for the underground verification of the construction and testing techniques. The plugs were constructed using wet-process sprayed SFRC with a high fibre content (90kg/m<sup>3</sup>) (Hilar and Pruška, 2011).

## 2. Description of the laboratory work

Since the simulation of unsaturated swelling materials is somewhat complicated and the EPSP underground laboratory experiment will not be dismantled during the course of the project, the construction of physical models of plugs at the laboratory scale (physical hydraulic model – PHM) was proposed in the laboratory work plan. The aim of these



experiments is to gain data for the subsequent calibration of numerical models of the saturation of the bentonite material. In all of the experiments synthetic granitic water is used and the bentonite material is the same as was used for the EPSP experiment.

The compacted bentonite sample in the physical hydraulic models was equipped with measurement sensors and subjected to gradual saturation. The results of the physical hydraulic model tests consisted of curves describing the development of:

- The volume of water which infiltrated into the sample
- The pressure under which the water infiltrated
- The development of relative humidity (RH) at the observation points
- The development of swelling pressure at the end of the sample

The aim of the PHMs was to describe the hydraulic and mechanical processes under way during the saturation of the bentonite. Two PHMs were constructed, one using bentonite powder and the other bentonite pellets. The two different materials were also chosen with respect to subsequent numerical modelling. Notably, the simulation of a laboratory experiment by means of numerical modelling using bentonite powder was found to be easier than simulation using bentonite pellets.

Both of the physical hydraulic models consisted of nine stainless steel chambers of cylindrical shape with approximate dimensions of 0.05m in length and 0.08m in diameter (the total length of the bentonite in the PHM is 45cm) and were equipped with RH sensors in order to record the distribution of water content within the bentonite material (Fig. 1 and Fig. 2).

Bentonite with bulk density of from 1 400kg/m<sup>3</sup> (the same bulk density as was used in the EPSP experiment) was pressed into the nine chambers and was gradually saturated with water under pressure. The level of water pressure was 2MPa as determined by the field testing of the permeability of grouted rock at the Josef Underground Laboratory. A sample of the bentonite material was removed following the conclusion of the experiment (approximately 1 year; after 450 days with regard to the PHM with bentonite powder and 380 days with respect to that with bentonite pellets) and divided into layers with an approximate thickness of 1cm. The water content in each layer was subsequently determined. The resulting data was added to the measured data concerning relative humidity and together they were compared to the retention curve derived by means of the block method applied to small samples.

The following data was recorded during the experimentation stage:

- The volume of water which infiltrated into the sample
- The pressure under which the water infiltrated
- The development of RH at observation points
- The development of swelling pressure at the end of the sample

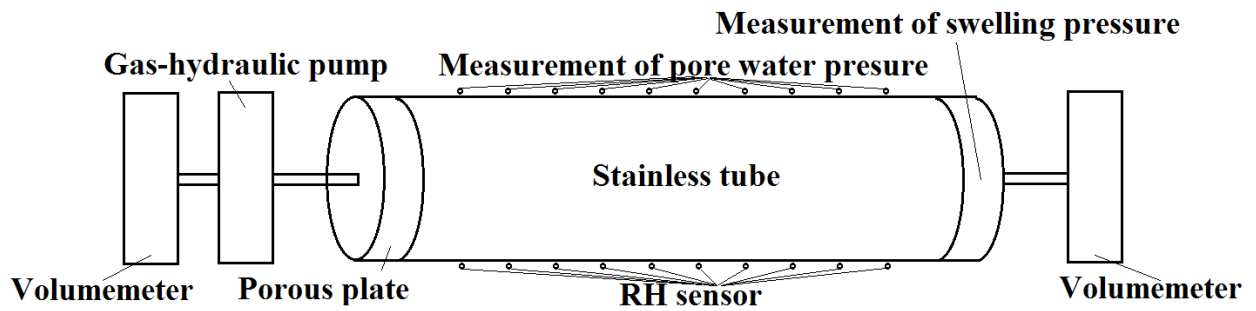


Fig. 1 The geometry of the physical hydraulic model

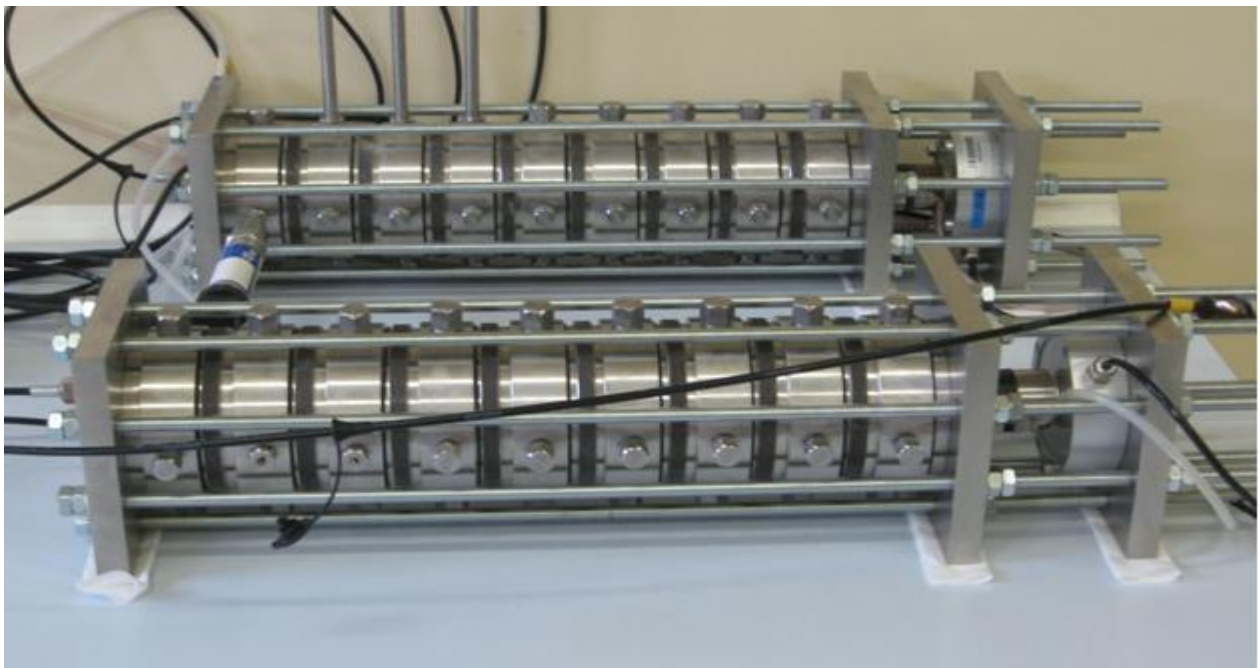


Fig. 2 Two physical hydraulic models - one filled with bentonite powder and the second with bentonite pellets.

The PHM with bentonite powder

The results of the physical hydraulic model tests using bentonite powder are shown in Fig. 3 to Fig. 5 from which it may be inferred that the saturation rate of the material decreases in the direction of flow.

Furthermore, it is apparent that the swelling pressure reaction is consistent with that of relative humidity at a distance of 2.5cm from the sensor for the measuring of swelling pressure (the distance between two sensors is 2.5cm).

The graphs show that it was possible to maintain constant conditions throughout the duration of the experiment with the exception of 3 days during which the pressure was reduced by 4 bar due to damage to the pressure reducing valve.

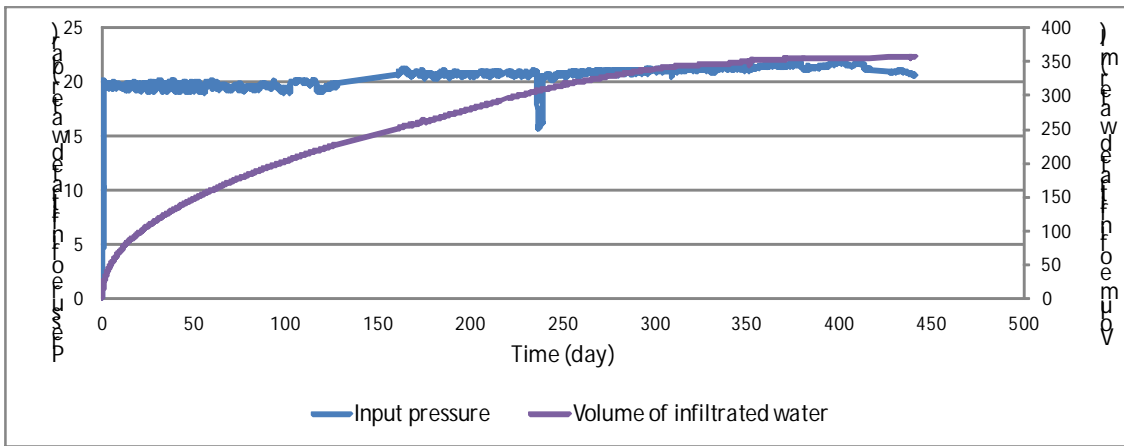


Fig. 3 The pressure and volume of water which infiltrated into the sample. The pressure drop after around 230 days was caused by the temporary failure of the pressure reducing valve.

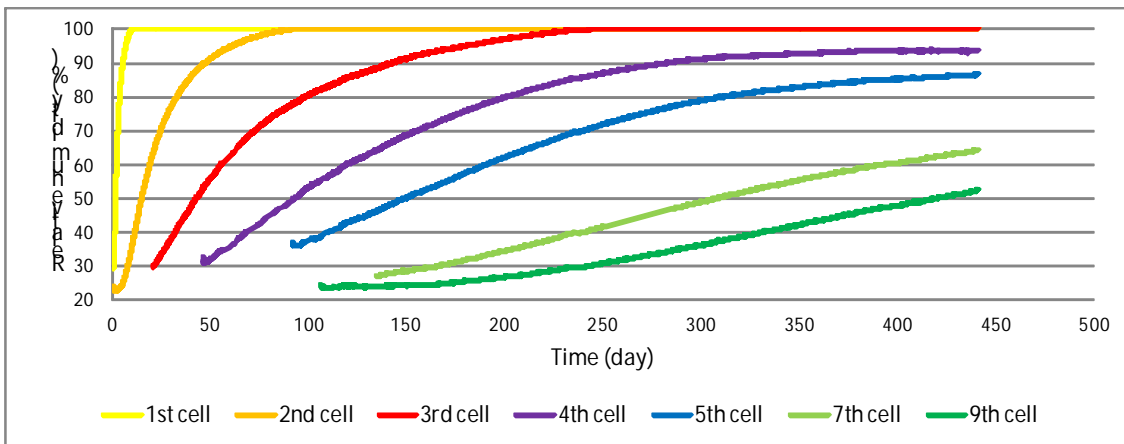


Fig. 4 Development of relative humidity at various observation points.

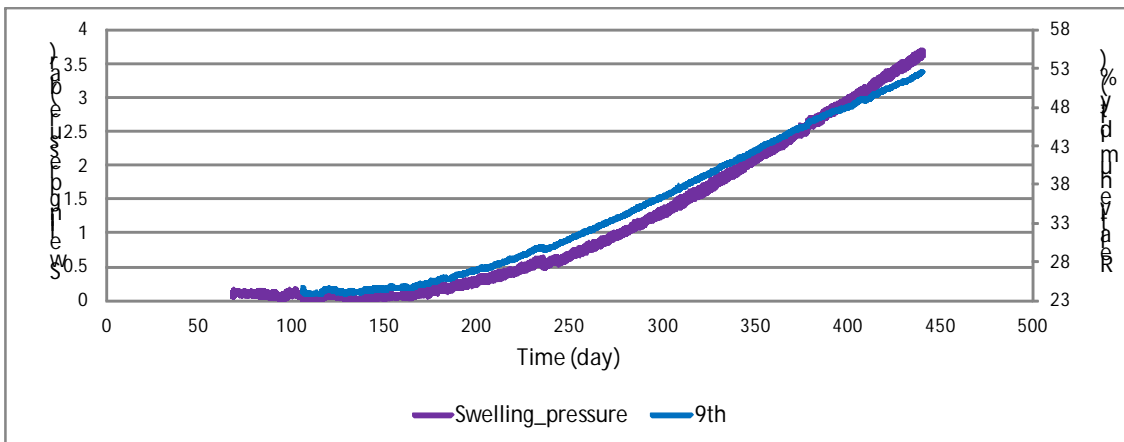


Fig. 5 Comparison of the development of swelling pressure and relative humidity at the 9th observation point.



After a period of around 450 days, the saturation of the bentonite was terminated and the physical model was dismantled into the form of individual cells (9 in total, Fig. 6). A 5cm cube of bentonite was extracted from each cell and cut into plates with an approximate thickness of 1cm (samples). Subsequently, the water content of each sample was determined; the resulting values are shown in Fig. 7.

A comparison of Fig. 4 and Fig. 7 shows that although the RH sensors show a value of 100%, the material is not fully saturated. This is due to the principle of the functionality of the RH sensor, i.e. the sensor is incapable of measuring the material in a state close to full saturation (Villar, 2007). Fig. 7 shows the gradual distribution of moisture with concern to which the state of the material at the beginning of the physical hydraulic model test is controlled by the condition/state of the material at the end of the test.



Fig. 6 The dismantling of the physical hydraulic model into individual cells.

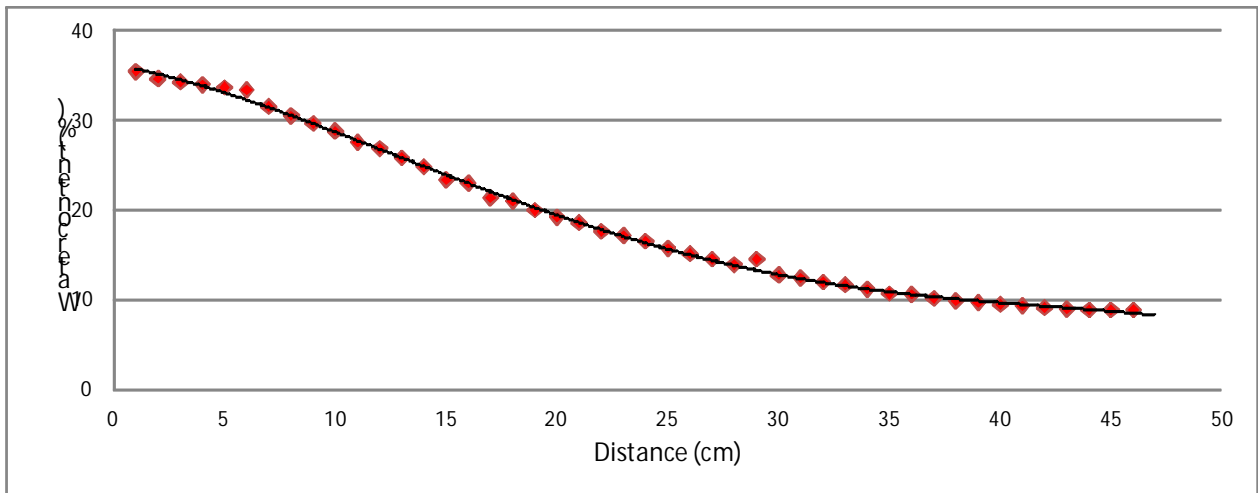


Fig. 7 Profile of mass water content in the PHM; the distance indicates the position of the samples from the beginning of the physical model.

The moisture retention curve was determined from the measured values of relative humidity (following conversion to suction pressure) and the corresponding water content and was then compared with the retention curve obtained by using the block method (Fig. 8). The results indicate that, despite the difference in scale (the block method sample had a volume of around  $53\text{cm}^3$ ), the retention curves match very well.

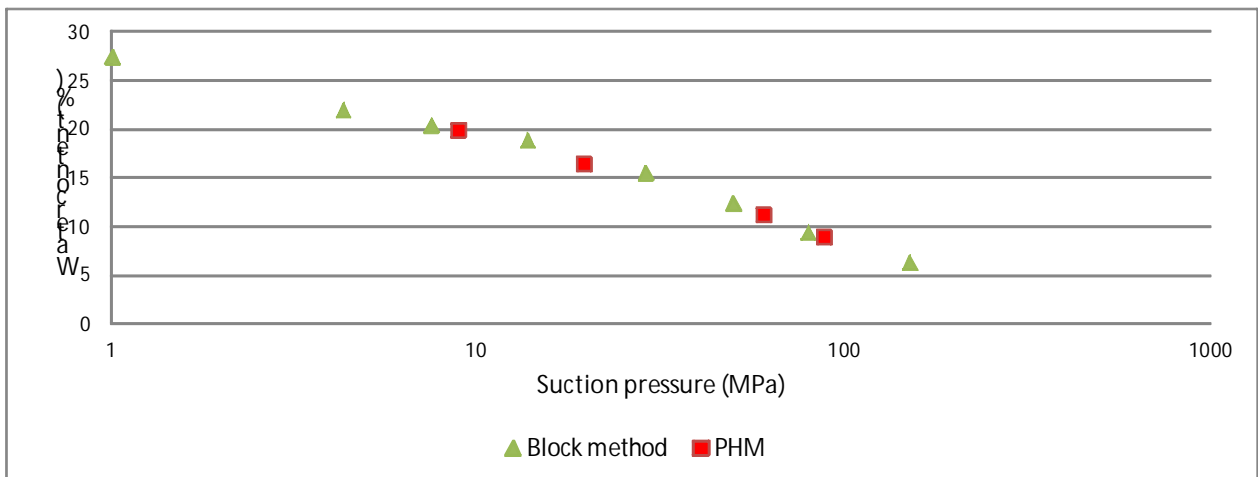


Fig. 8 Comparison of the retention curves of bentonite B75 obtained via the block method and following the dismantling of the physical hydraulic model.

The PHM with bentonite pellets

The physical hydraulic model using bentonite pellets had the same geometry as the physical hydraulic model using bentonite powder. Because of the requirement for even and continuous saturation, the first cell of the model contained a 5cm-thick layer of bentonite powder compacted to a dry bulk density value of  $1400\text{kg/m}^3$  so as to avoid the suffusion of the void spaces (which necessarily exist between bentonite pellets) by pressurised water and which



simulates a layer with low permeability such as that provided by concrete. The second to ninth cells of the model contained bentonite pellets.

The resulting data, illustrated in Fig. 9 to Fig. 11, reveals the same processes as those observed in the physical hydraulic model using bentonite powder. The saturation rate of the material decreases in the direction of flow and the reaction of swelling pressure is consistent with that of relative humidity at a distance of 2.5cm from the sensor for the measuring of swelling pressure (the distance between two sensors is 2.5cm).

With respect to the physical hydraulic model using bentonite pellets, constant conditions were maintained throughout the whole duration of the experiment. Notably, the sensor in the fifth cell ceased to function during the course of the experiment.

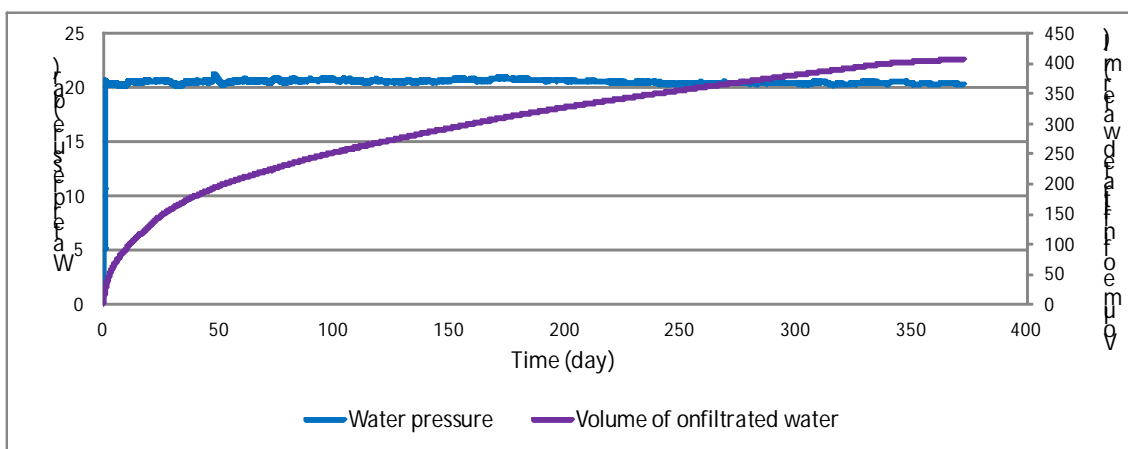


Fig. 9 Pressure and volume of the water which infiltrated into the sample.

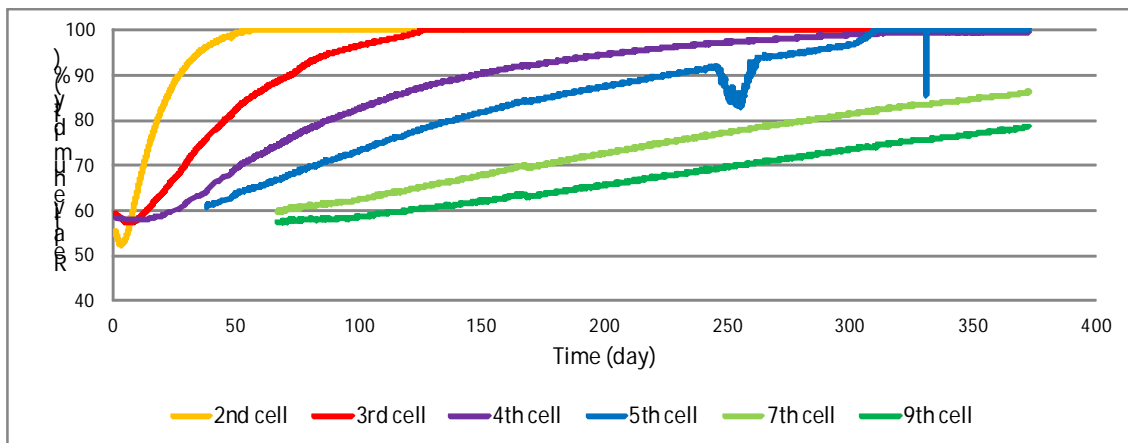


Fig. 10 Development of relative humidity at different observation points. The sensor at the fifth observation point ceased to function during the experiment.

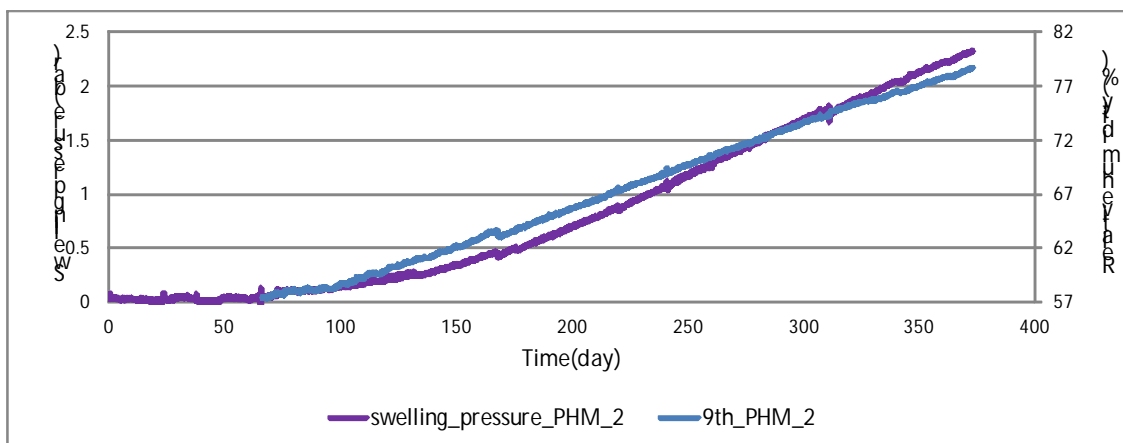


Fig. 11 Comparison of the development of swelling pressure and relative humidity at the 9th observation point.

Following a period of around 380 days, the saturation of the bentonite was terminated and the physical model dismantled into its individual cells (9 in total). A block of bentonite was then extracted from each cell and cut into plates with an approximate thickness of 1cm (samples). Subsequently, the water content of each sample was determined; the results are shown in Fig. 12.

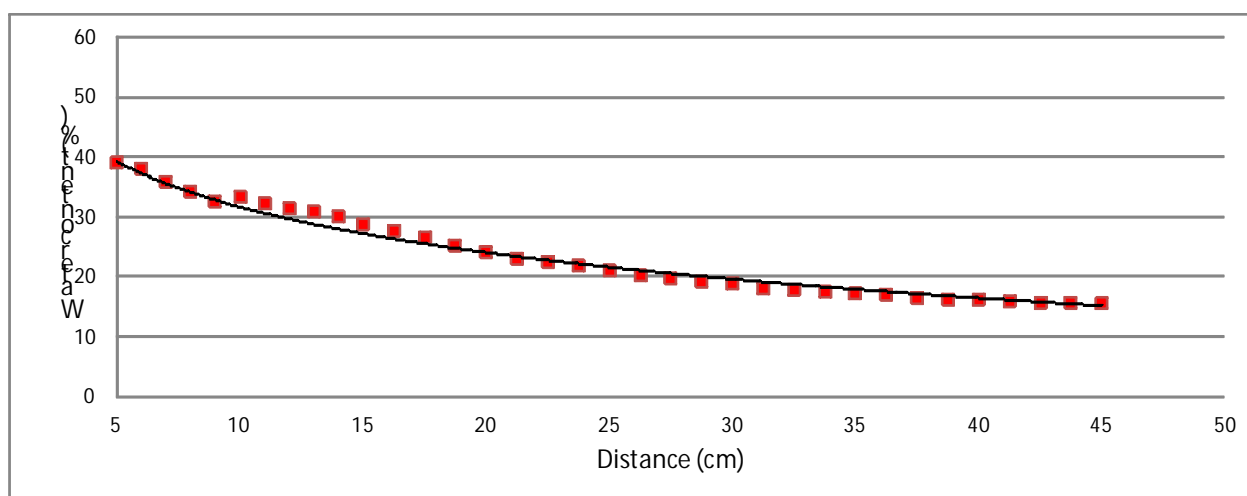


Fig. 12 Profile of mass water content in the PHM using bentonite pellets; the distance indicates the position of the samples in relation to the beginning of the physical model

### 3. Numerical modelling

#### 3.1 Computer software employed

CODE\_BRIGHT consists of a Finite Element Method (FEM) program capable of performing coupled thermo-hydro-mechanical (THM) analysis in geological media. It was developed by the Department of Geotechnical Engineering and Geo-Sciences of the Polytechnic University



of Catalonia (UPC), and works in combination with pre/post-processor GiD, developed by the International Centre for Numerical Methods in Engineering (CIMNE).

### 3.2 Conceptual model

The model addresses the HM (hydro-mechanical) response of a highly-compacted bentonite barrier. The HM-coupled analysis was performed using a 2-D axi-symmetric longitudinal section. The model has a rectangular shape with dimensions of 0.04 x 0.45m and the surface area is covered by a uniformly structured grid. The grid step distance is 0.5cm which means 8 points in the  $x$  direction and 90 points in the  $y$  direction.

The HM analysis takes into account the following phenomena:

1. Water flow: the liquid phase (Darcy's law) and water vapour diffusion (Fick's law)
2. Mechanical behaviour: the behaviour of the bentonite depends on suction and stress

The HM version of the Barcelona Basic Model (BBM) was employed in the analysis in connection with mechanical behaviour. The models take into account the stress-stiffness with suction variation and that of swelling potential with stress and suction so as to reproduce the swelling behaviour of bentonite taking into account the high level of compaction to which the bentonite blocks were subjected.

Fig. 13 and Fig. 14 present the various parameters together with the constitutive laws that were used as the initial parameters, which were taken principally from FEBEX reports (UPC, 2015).



<b>MECHANICAL DATA</b>	
Termo elasto-plastic (TEP): Elastic parameters	
ITYCL	1
P1: $\kappa_{i0}$	0.05
P2: $\kappa_{s0}$	0.30
P3: $K_{min}$ (MPa)	0.1
P5: $\nu$	0.4
P8: $\alpha_i$	-0.003
P9: $\alpha_{sp}$	-0.147
P10: $p_{ref}$ (MPa)	0.01
Termo elasto-plastic (TEP): Thermal parameters	
ITYCL	1
P1: $\alpha_\theta$	1.5E-4
P5: $T_{ref}$	20
Termo elasto-plastic (TEP): Plastic parameters (1)	
ITYCL	1
P1: $\lambda(0)$	0.15
P2: $r$	0.75
P3: $\beta$ (MPa <sup>-1</sup> )	0.05
P4: $\rho$ (°C <sup>-1</sup> )	0.2
P5: $k$	0.1
P6: $p_{s0}$ (MPa)	0.1
Termo elasto-plastic (TEP): Plastic parameters (2)	
ITYCL	1
P1: $p^c$ (MPa)	0.1
P2: $M$	1.0
P3: $\alpha$	0.3
P4: $e_0$	0.6
P5: $p_0^*$ (MPa)	14

$$d\varepsilon_v^e = \frac{k_i(s)}{1+e} \frac{dp'}{p'} + \frac{k_s(p',s)}{1+e} \frac{ds}{s+0.1} + (\alpha_o)dT$$

where:

$$k_i(s) = k_{io} (1 + \alpha_i s)$$

$$k_s(p',s) = k_{so} (1 + \alpha_{sp} \ln p' / p_{ref})$$

$$p_o = p^c \left( \frac{p_o^*(T)}{p^c} \right)^{\frac{\lambda(o)-kio}{\lambda(s)-kio}}$$

$$p_o^*(T) = p_o^*$$

$$\lambda(s) = \lambda(o) [(1-r) \exp(-\beta s) + r]$$

$$p_s = p_{s0} + ks \exp(-\rho \Delta T)$$

$$\Delta T = T - T_{ref}$$



Termo elasto-plastic (TEP): Parameters shape yield surface	$g_y(\theta)=1$
ITYCL 3	
Termo elasto-plastic (TEP): Parameters shape plastic potential	$g_p(\theta)=1$
ITYCL 3	
Termo elasto-plastic (TEP): Integration control parameters	
ITYCL 1	
P1: <i>Tole1</i> 1.E-8	
P2: <i>Tole2</i> 1.E-3	
P3: <i>Tole2</i> 1.E-3	
P4: $\mu$ 1	
P5: <i>Index</i> -1	

Fig. 13 Initial model parameters describing the mechanical data (UPC, 2015); individual values are explained in UPC (2015a).

<b>HYDRAULIC AND THERMAL DATA</b>	
Retention Curve:	Van Genuchten model:
ITYCL 1	$S_e = \frac{S_l - S_{rl}}{S_{lz} - S_{rl}} = \left( 1 + \left( \frac{P_g - P_l}{P} \right)^{\frac{1}{1-\lambda}} \right)^{-\lambda}$ $P = P_o \frac{\sigma}{\sigma_o}$
P1: $P_o$ (MPa) 20	
P2: $\sigma_o$ (N m <sup>-1</sup> ) 0.072	
P3: $\lambda$ 0.18	
P4: $S_{rl}$ 0.01	
P5: $S_{lz}$ 1	
Intrinsic Permeability:	Darcy's law:
ITYCL 1	$\mathbf{q}_l = -\frac{\mathbf{k}k_{rl}}{\mu_l} (\nabla P_l - \rho_l \mathbf{g})$ Kozeny's model: $\mathbf{k} = \mathbf{k}_o \frac{\phi^3}{(1-\phi)^2} \frac{(1-\phi_o)^2}{\phi_o^3}$
P1: $(k_{11})_o$ (m <sup>2</sup> ) 5.E-21	
P2: $(k_{22})_o$ (m <sup>2</sup> ) 5.E-21	
P3: $(k_{33})_o$ (m <sup>2</sup> ) 5.E-21	
P4: $\phi_o$ 0.4	
P5: $\phi_{min}$ 0.001	
Liquid phase relative Permeability:	
ITYCL 6	$k_{rl} = AS_e^\lambda$
P2: $A$ 1	
P3: $\lambda$ 3	
<b>PHASE PROPERTIES</b>	
Solid phase	
ITYCL 1	
P1: $C_s$ (J kg <sup>-1</sup> K <sup>-1</sup> ) 1000	
P2: $\rho_s$ (kg m <sup>-3</sup> ) 2770	
P3: $\alpha_s$ (°C <sup>-1</sup> ) 7.8E-6	

Fig. 14 Initial model parameters describing the hydraulic and thermal data and phase properties (UPC, 2015).



The main process under way in the PHMs consisted of pressurised saturation under controlled conditions. The testing procedure involved:

1. An initial hydration phase during which the bentonite was flooded with water under zero pressure so as to allow the closure of the joints between the bentonite blocks. The duration of this initial phase was 1 day in both the PHM using bentonite powder and that using bentonite pellets.
2. Once the initial hydration phase had been completed, the process commenced involving test saturation under pressure for the duration of the testing stage (about one year).

This procedure was taken into account in terms of determining the flux boundary condition as described below. Since this is an HM-related issue, it was necessary to define the following conditions:

- Mechanical boundary conditions
- Flux boundary conditions
- Initial unknowns
- Initial stress
- Initial porosity

***Mechanical boundary conditions:***

In order to take into account that the main body of the cylinder consisted of a stainless steel cell, the assumption of null displacement was prescribed for the outer boundaries as follows:

1. The restriction of vertical displacement along the horizontal boundaries (perpendicular to the wall of the cell)
2. The restriction of horizontal displacement along the vertical boundaries

***Hydraulic boundary condition:***

A water pressure level of 2MPa was prescribed for the lower horizontal boundary so as to simulate the hydration of the bentonite. A seepage face condition was prescribed for the upper horizontal boundary.

***Initial unknowns:***

The principal initial unknown consisted of the water pressure within the model prior to the commencement of saturation. An initial value of suction of -192MPa was adopted for the PHM using bentonite powder and -80MPa for that using bentonite pellets. These values were taken from RH sensors and were converted to pore water pressure using the Kelvin equation (1)

$$s = -10^{-6} \frac{R \times T}{V_w} \ln \left( \frac{RH}{100} \right), \quad (1)$$

where  $R$  is the universal gas constant,  $T$  is absolute temperature,  $V_w$  is the molar volume of water and  $RH$  the relative humidity.

***Initial Stress:***

A constant hydrostatic value of 0.11MPa was adopted as the initial stress value within the bentonite material.

***Initial Porosity***

The initial porosity of the bentonite was considered equal to 0.5.



### *Time interval*

The duration of the computed task was determined as the duration of the laboratory experiments, i.e. 450 days in the case of the bentonite powder model and 380 days in that of the bentonite pellet model.

## **4. Calibration of the numerical model**

### **4.1 Numerical model of the PHM using bentonite powder**

The data gathered from the laboratory experiments (namely the volume of infiltrated water and the development of relative humidity recalculated to pore water pressure) formed the basis for model calibration. Furthermore, the model retention curve and the curve determined from the laboratory tests were compared. The prescribing of a larger number of calibration criteria reduces the degree of freedom of the numerical solution wherein the model is able to achieve the same result via different combinations of model parameters.

Due to the large number of model parameters, retention curve parameters (P1, P3) and hydraulic conductivity ( $P1 = P2 = P3$ ) were the only parameters adopted in terms of describing saturation for calibration purposes. Thus, the change in model results was observed depending on the change in just three model parameters.

The resulting parameters for the test using bentonite powder are listed in Tab. 1, a comparison of the measured and modelled values of the development of the volume of infiltrated water is shown in Fig. 15, a comparison of the development of water pressure at individual observation points is shown in

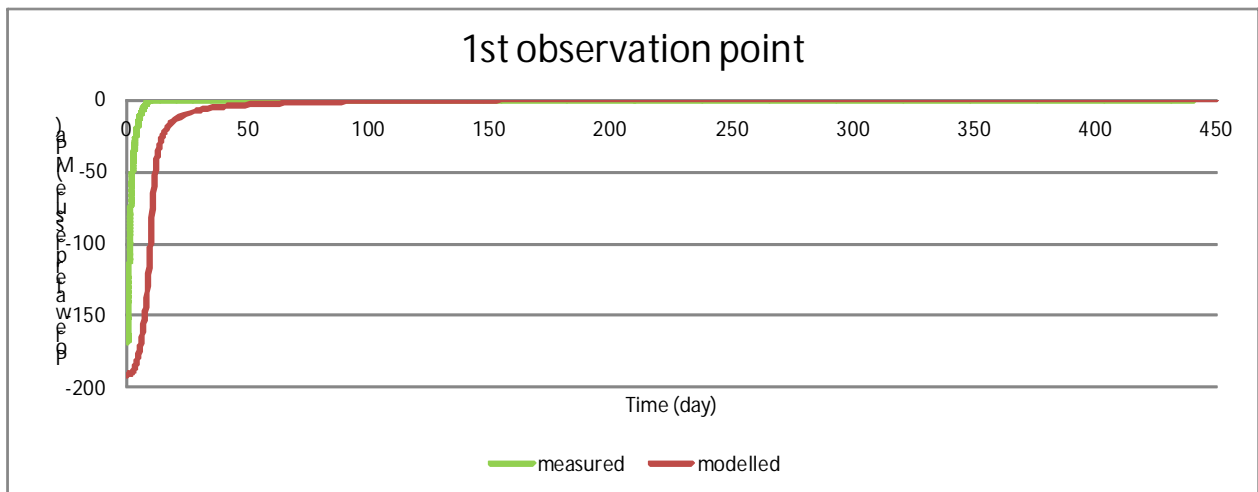


Fig. 16 -

Fig. 22, and the conformity of the model and the measured retention curves is shown in Fig. 23.



Tab. 1 The model parameters describing hydraulic data in the model using bentonite powder. Individual values and their units are explained in UPC (2015a).

Parameters	ITYCL	P1	P2	P3	P4	P5
Retention curve	1	20	0.072	0.27	0.001	1
Intrinsic permeability	1	5.E-21	5.E-21	5.E-21	5.E-01	0

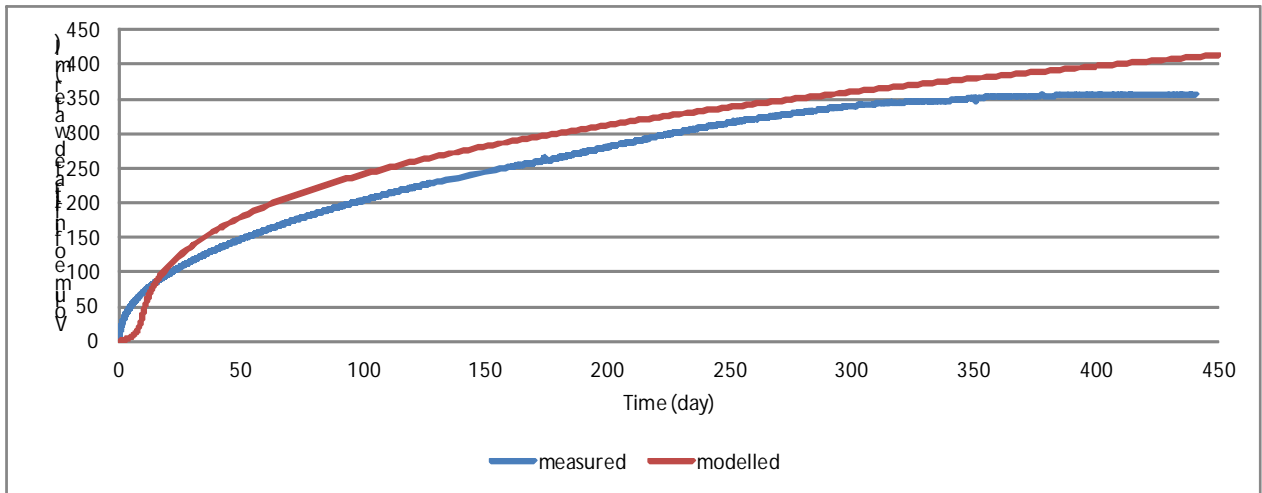


Fig. 15 Comparison of model and measured values of the volume of water which infiltrated into the bentonite powder sample

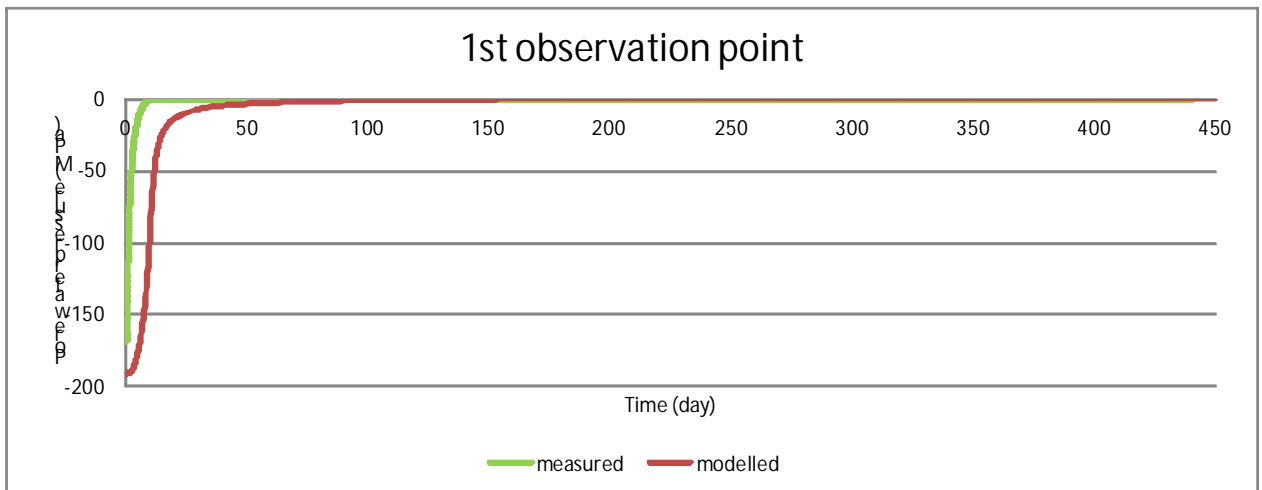


Fig. 16 Comparison of model and measured water pressure values at the 1st observation point

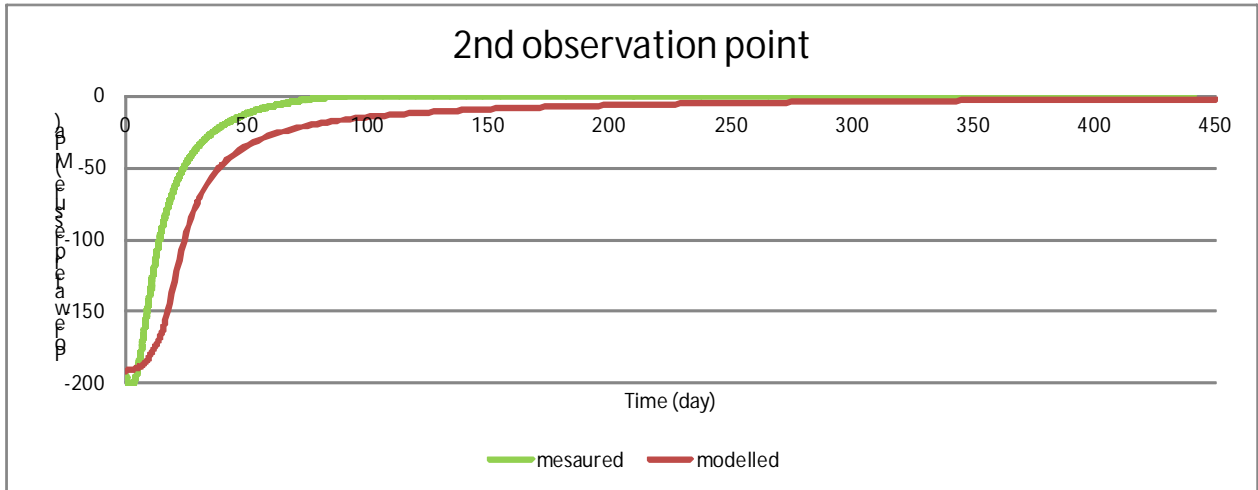


Fig. 17 Comparison of model and measured water pressure values at the 2nd observation point

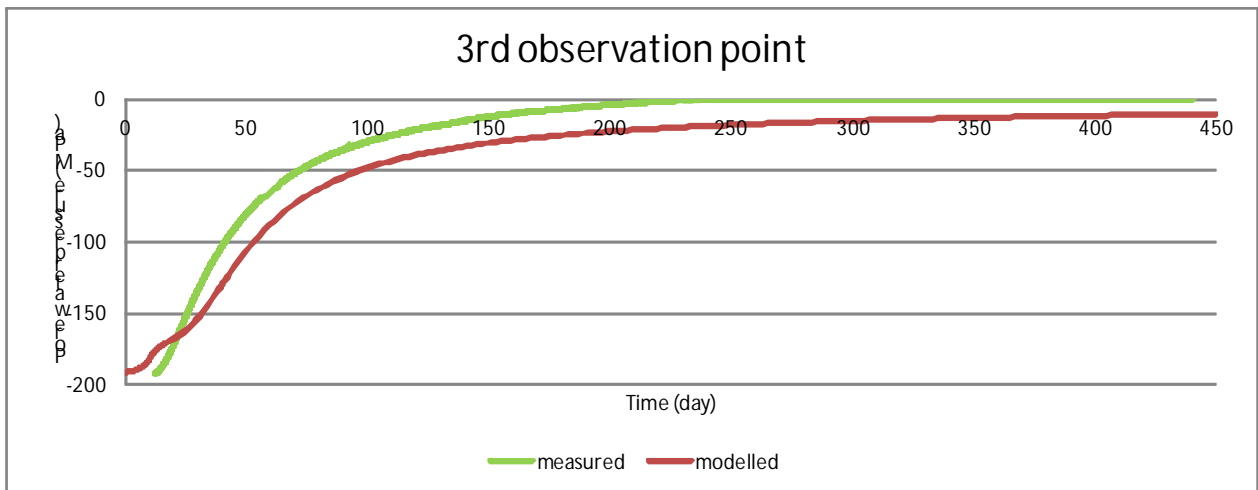


Fig. 18 Comparison of model and measured water pressure values at the 3rd observation point

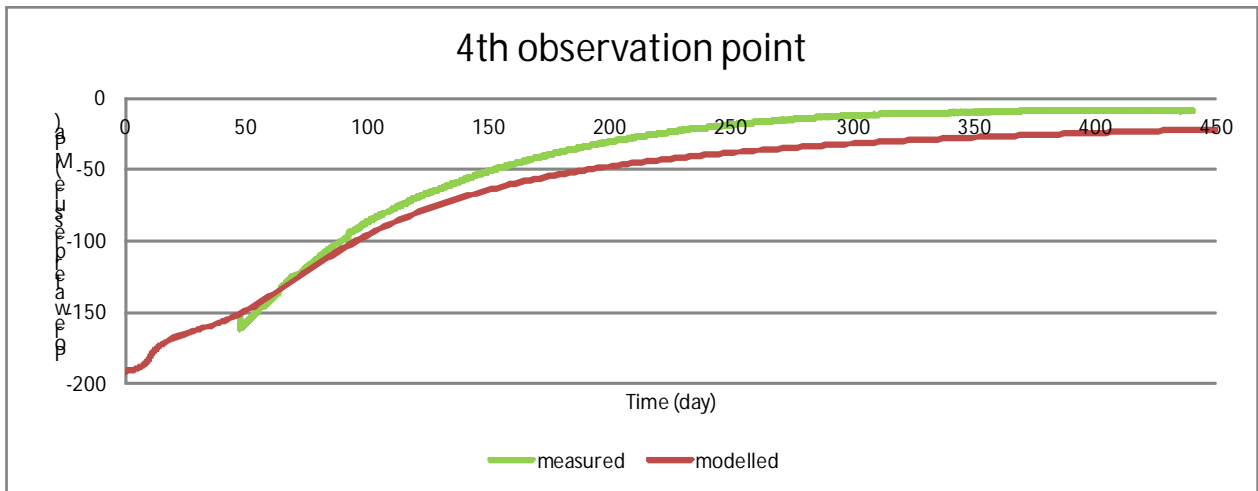


Fig. 19 Comparison of model and measured water pressure values at the 4th observation point

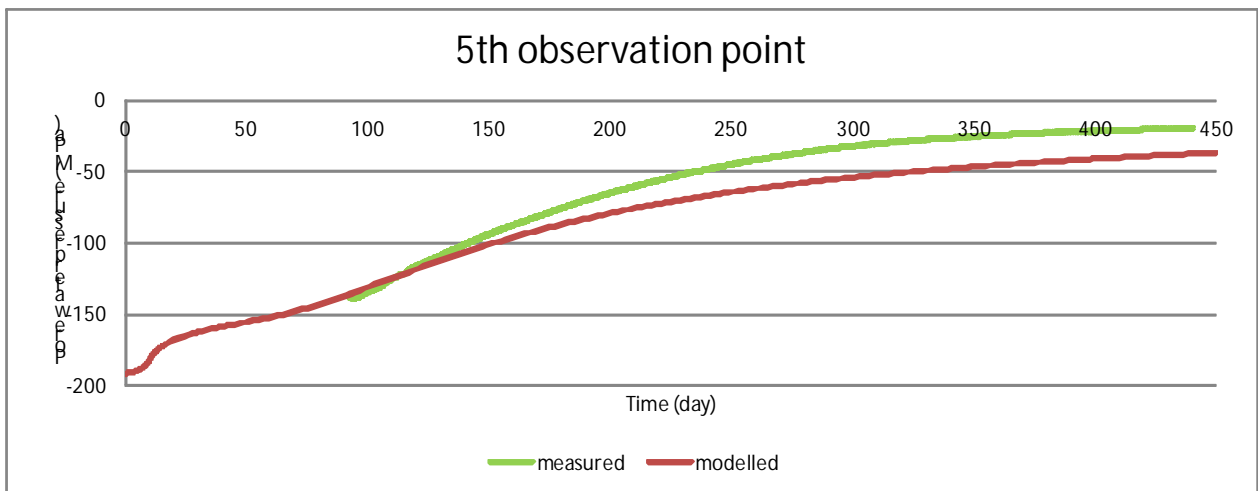


Fig. 20 Comparison of model and measured water pressure values at the 5th observation point

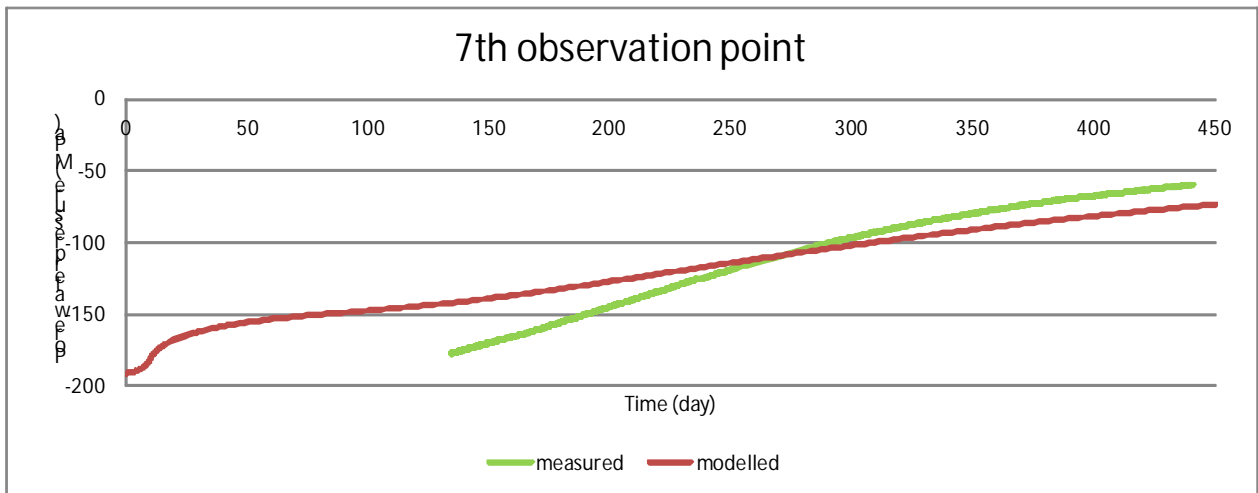


Fig. 21 Comparison of model and measured water pressure values at the 7th observation point

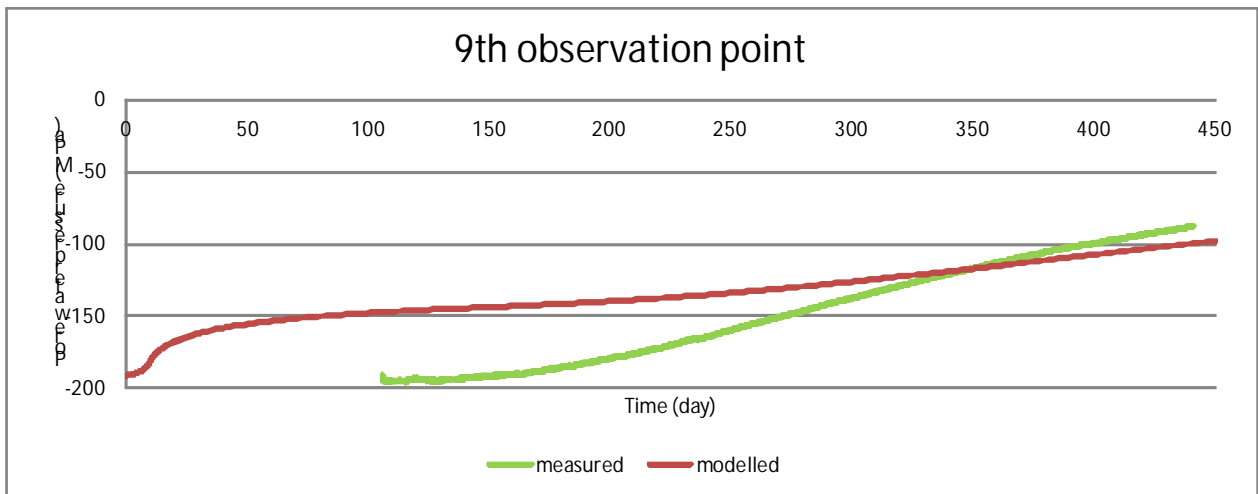


Fig. 22 Comparison of model and measured water pressure values at the 9th observation point

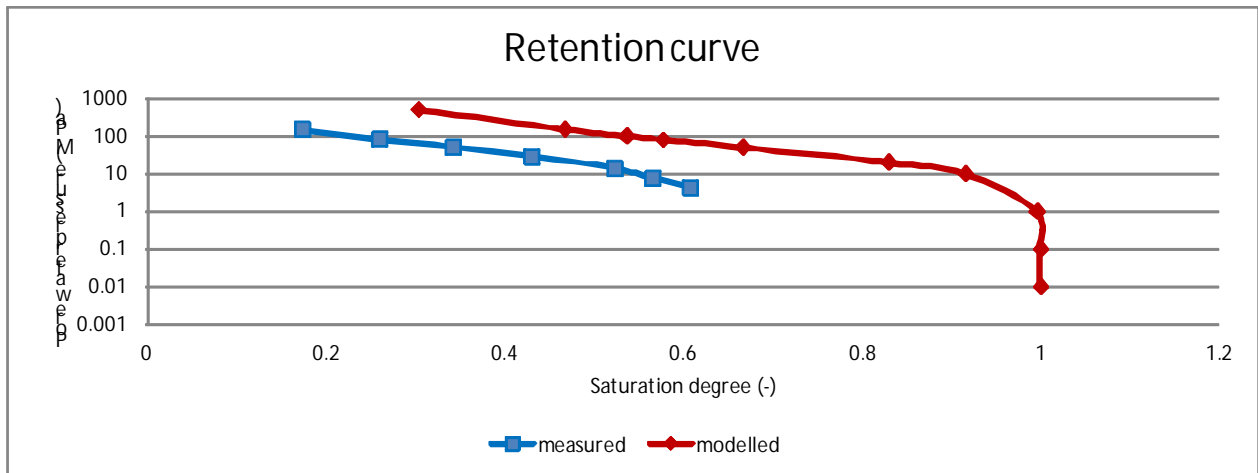


Fig. 23 Comparison of the model and measured retention curves

A comparison of the development of water pressure at the individual observation points reveals that the agreement of modelled and measured values decreases with distance from the point of saturation, especially at the beginning of the experiment. It was possible to achieve a better match for each of the calibration criteria separately during the calibration process; however, with increasing agreement with respect to one criterion, the degree of agreement decreased with regard to the other two criteria. If compliance was required with respect to all 3 calibration criteria, it was necessary to disregard perfect agreement between the measured and modelled values.

The calibrated parameters were employed for predictive modelling purposes with regard to which the most important question consisted of the expected time necessary for the complete saturation of a 45cm-long bentonite sample. Fig. 24 and Fig. 25 reveal that output from the second end of the model and the disappearance of negative capillary pressure occurred after a period of 2992.4 days.

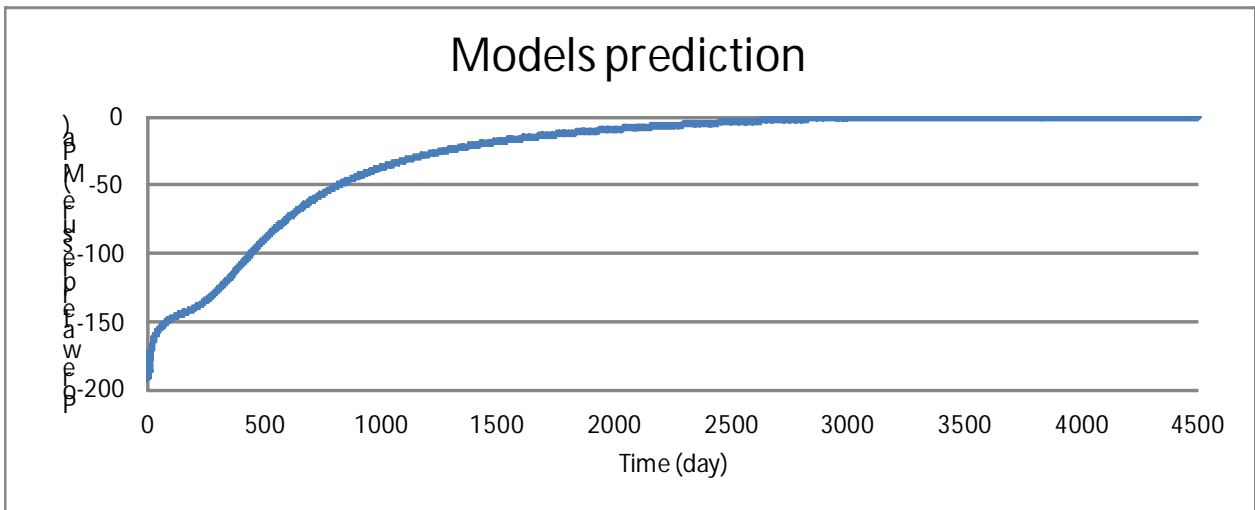


Fig. 24 Model prediction of the development of water pressure at the end of the bentonite sample

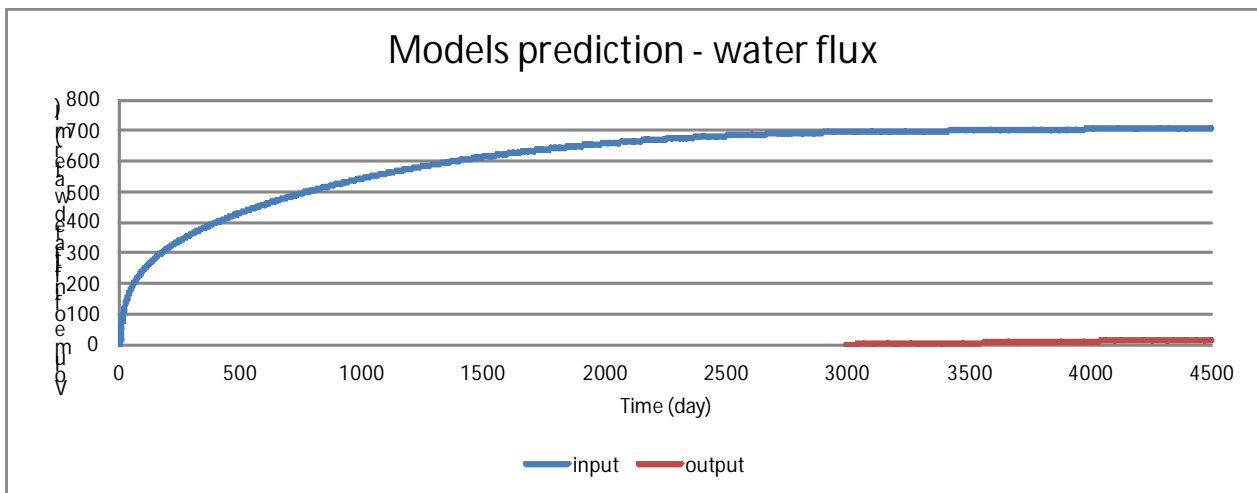


Fig. 25 Model prediction of the development of water balance at the beginning and end of the bentonite sample

#### 4.2 Numerical model of a PHM using bentonite pellets

The same criteria as those employed for the calibration of the model using bentonite powder were used for the calibration of the model using bentonite pellets

1. Volume of infiltrated water
2. Water pressure at each observation point
3. Retention curve

The structure of the pellets was not taken into account during the simulation of the bentonite pellet model, i.e. the material was considered to be homogeneous and the presence of pellets is assumed throughout the whole volume of the model.



The same model parameters as those used for the calibration of the bentonite powder model were entered into the calibration of the bentonite pellet model, i.e. retention curve parameters (P1, P3) and hydraulic conductivity (P1 = P2 = P3). It was observed that changes in the results of the model depend on a change in all three model parameters.

The resulting parameters with respect to the bentonite pellets experiment are listed in Tab. 1, a comparison of the measured and modelled values of the development of the volume of infiltrated water is shown in Fig. 26, a comparison of the development of water pressure at individual observation points is shown in

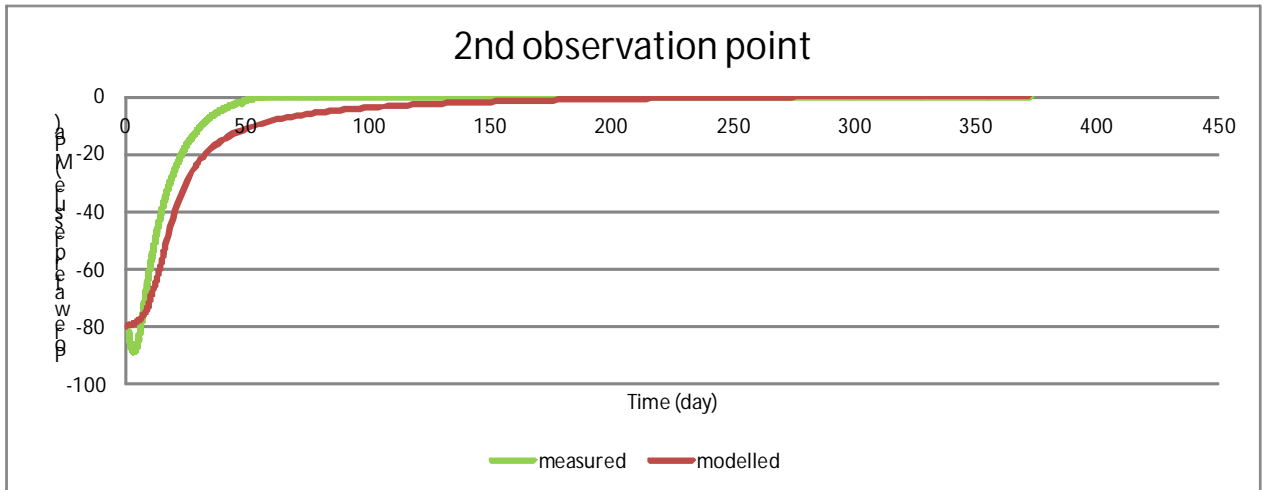


Fig. 27 -

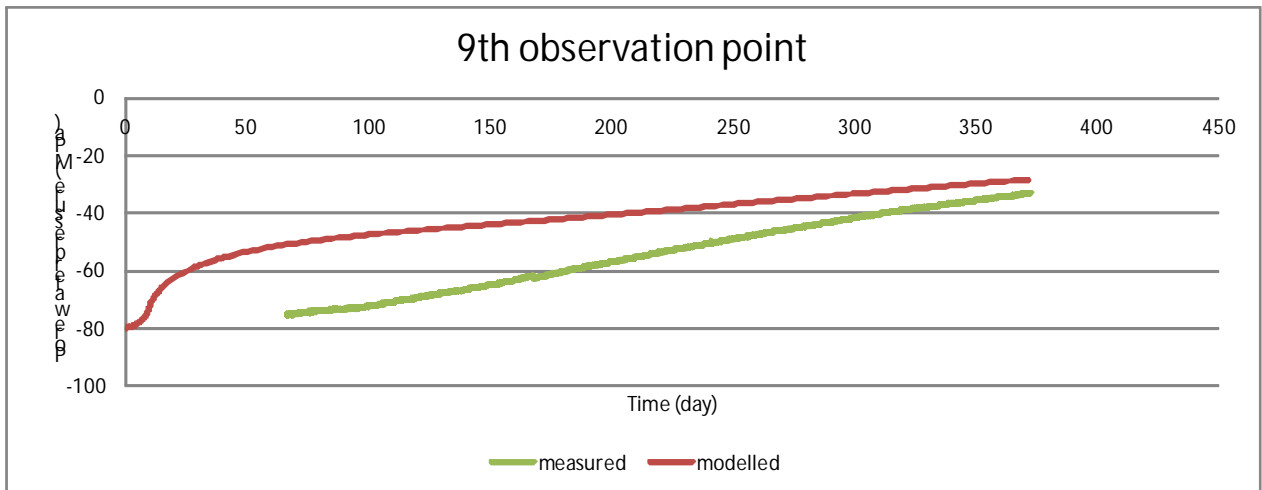


Fig. 32, and the conformity of the measured and modelled retention curves is shown in Fig. 34.

Tab. 2 The model parameters describing hydraulic data in the model using bentonite pellets. Individual values and units are explained in UPC (2015a).

Parameters	ITYCL	P1	P2	P3	P4	P5
------------	-------	----	----	----	----	----



Retention curve	1	10	0.072	0.22	0.001	1
Intrinsic permeability	1	1.E-20	1.E-20	1.E-20	5.E-01	0

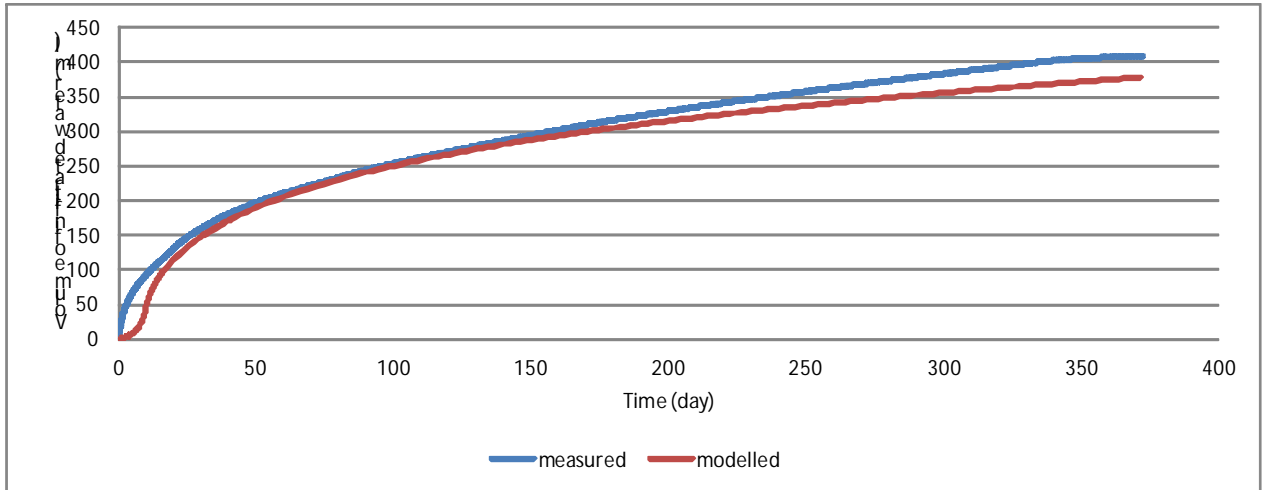


Fig. 26 Comparison of the model and measured values of the volume of water that infiltrated into the bentonite pellet sample

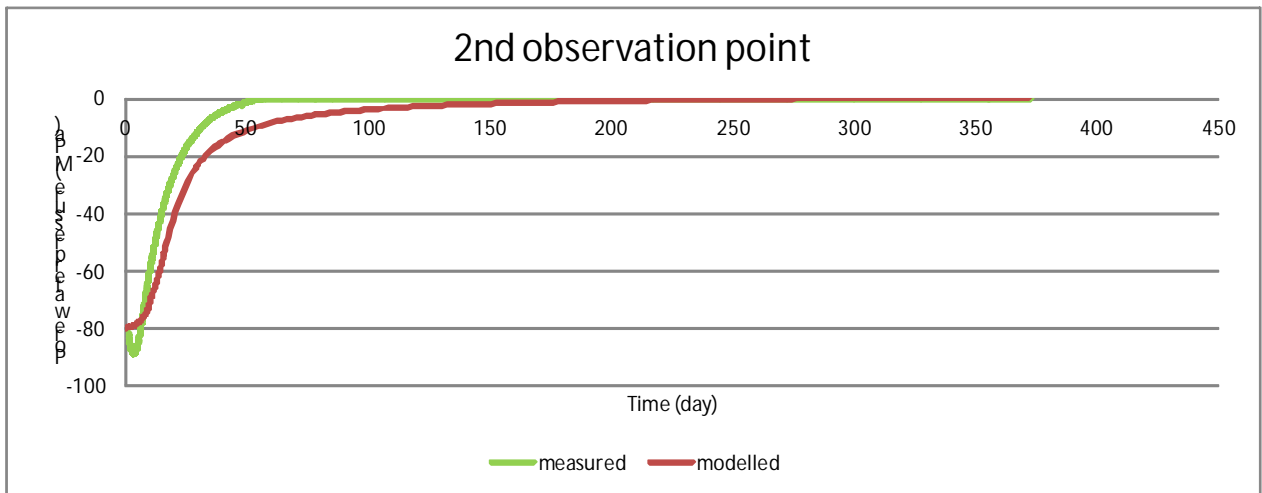


Fig. 27 Comparison of model and measured water pressure values at the 2nd observation point

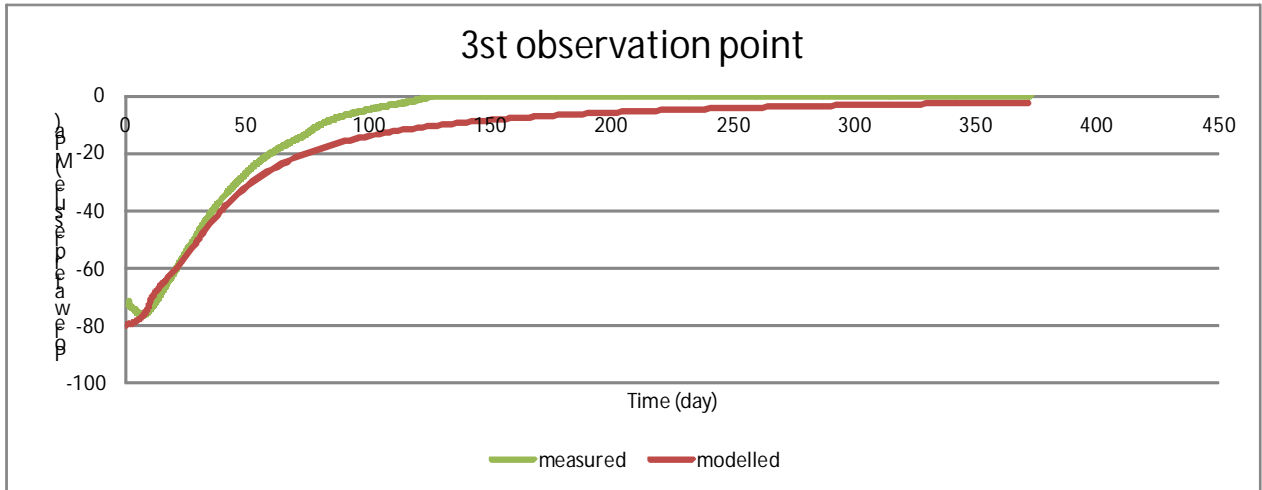


Fig. 28 Comparison of model and measured water pressure values at the 3rd observation point

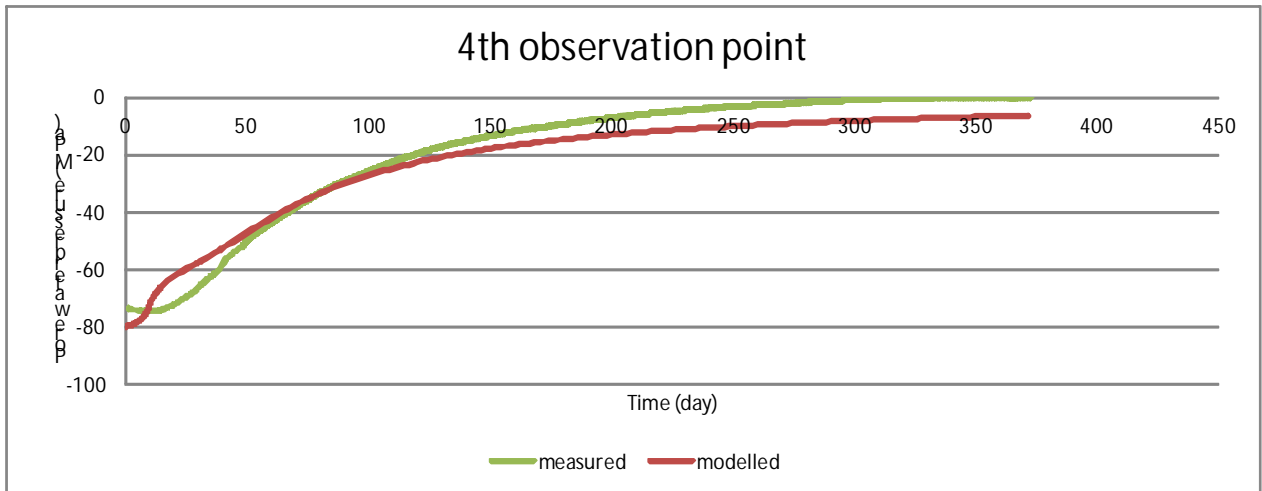


Fig. 29 Comparison of model and measured water pressure values at the 4th observation point

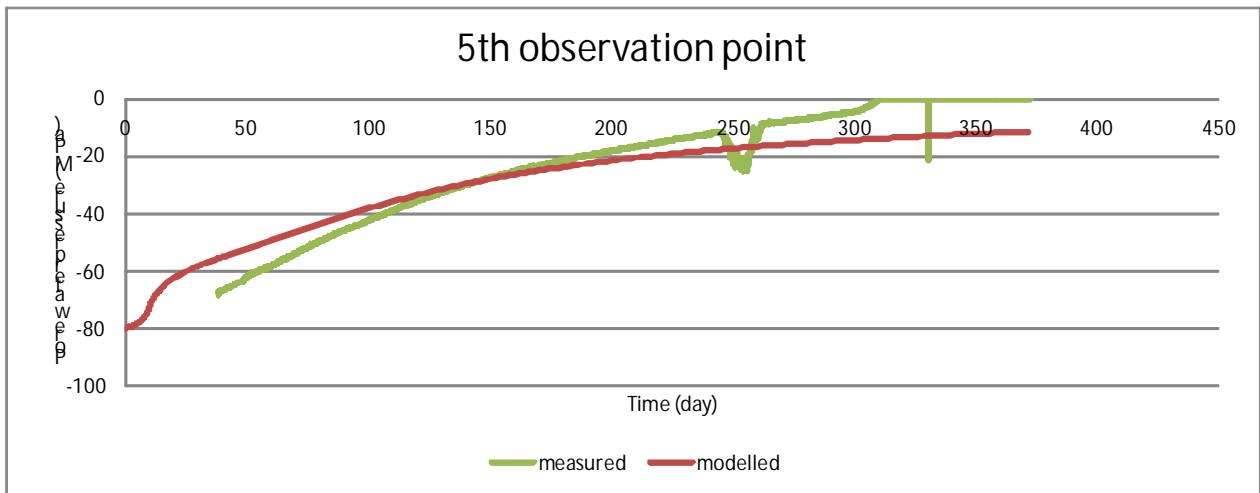


Fig. 30 Comparison of model and measured water pressure values at the 5th observation point. The sensor at the fifth observation point was damaged during the experiment.

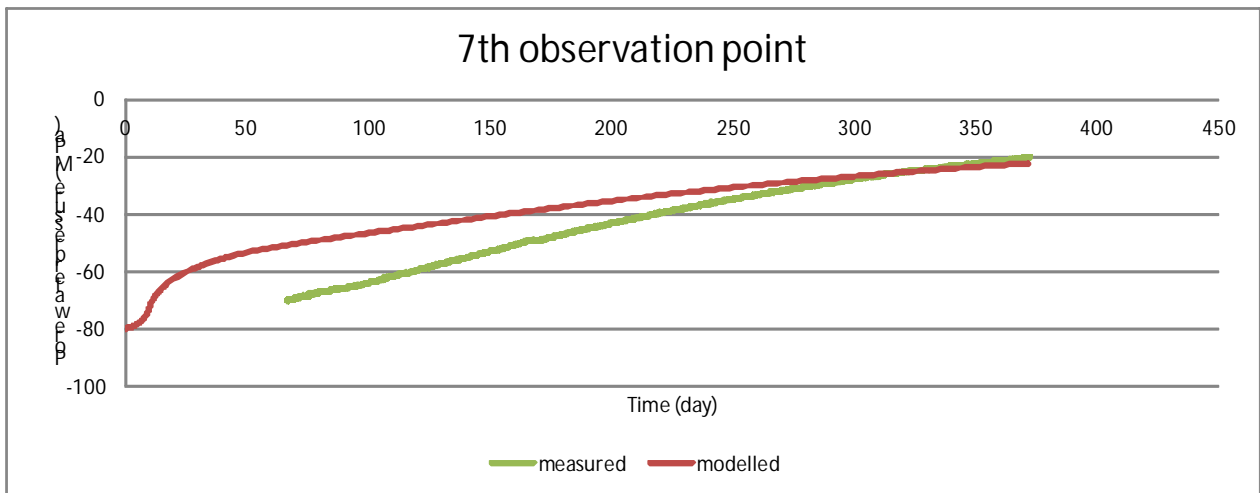


Fig. 31 Comparison of model and measured water pressure values at the 7th observation point

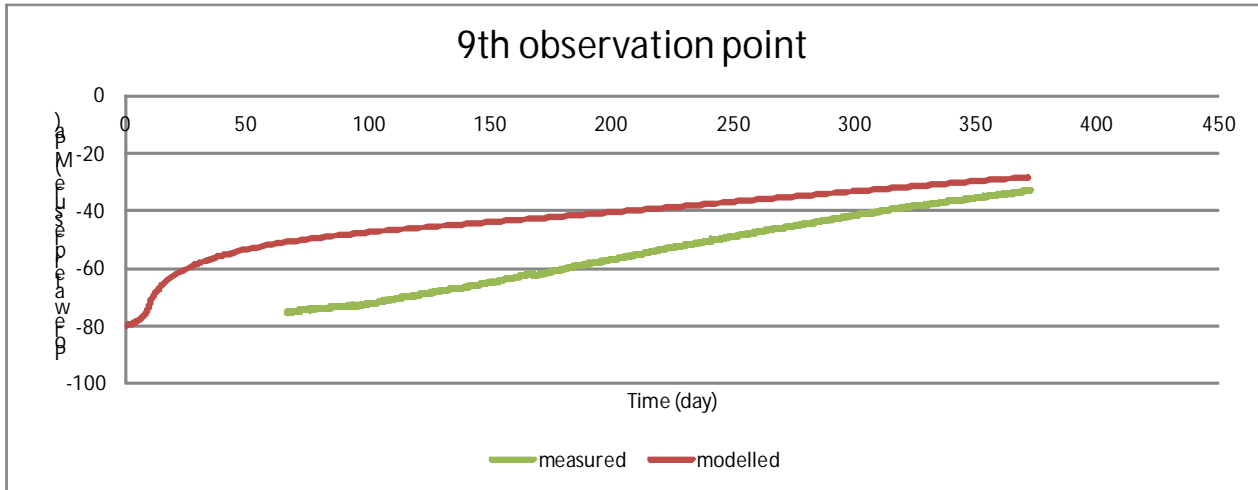


Fig. 32 Comparison of model and measured water pressure values at the 9th observation point

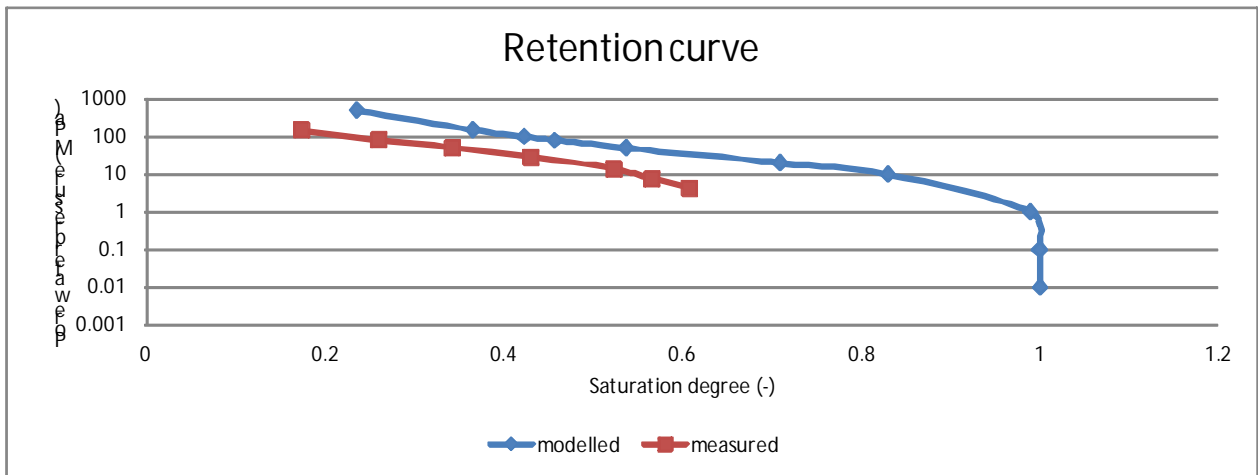


Fig. 33 Comparison of the model and measured retention curves

A higher degree of agreement between the measured and model results was achieved with respect to calibration according to the bentonite pellet PHM than that using bentonite powder.

The calibrated parameters were used for predictive modelling purposes, with respect to which the most important question was, again, the time required for the complete saturation of a 45cm-long bentonite sample. Fig. 34 and Fig. 35 show that output from the second end of the model and the cessation of negative capillary pressure occurred after 1833.8 days, i.e. around two-thirds of the time necessary for the complete saturation of the bentonite powder. However, it is important to note that the initial degree of saturation of the bentonite pellets was higher than that with regard to the saturation of the bentonite powder (the initial water pressure of the bentonite powder was -192MPa whilst that of the bentonite pellets was -80MPa).

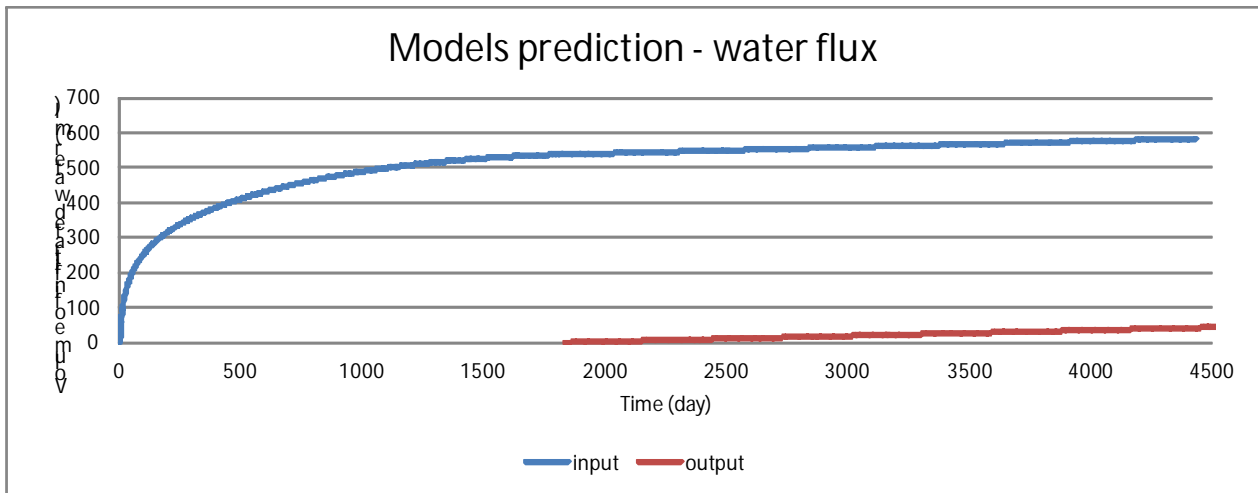


Fig. 34 Model prediction of the development of water balance at the beginning and end of the bentonite sample

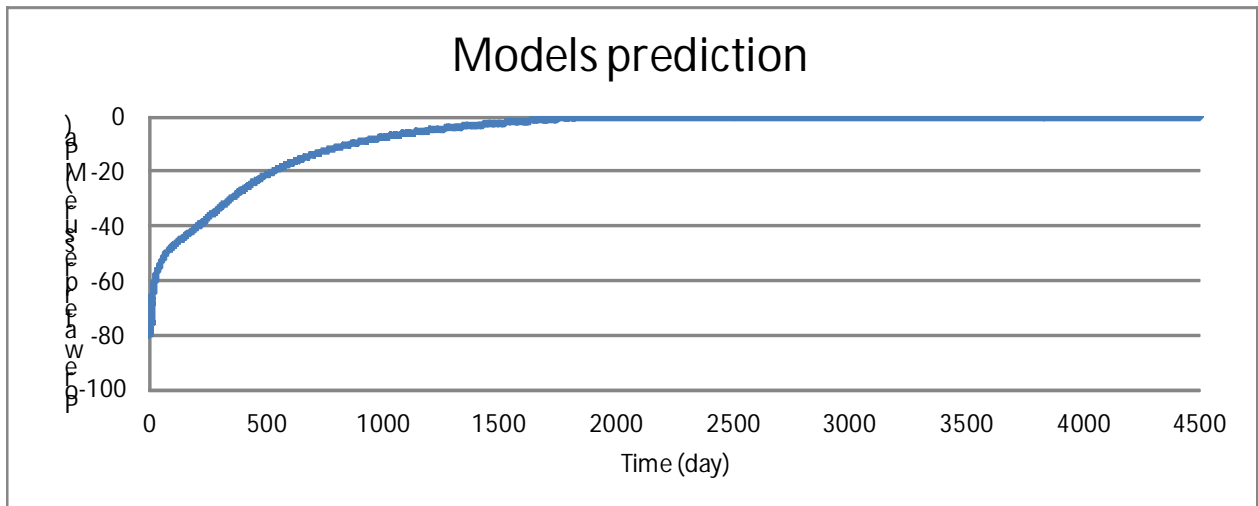


Fig. 35 Model prediction of the development of water pressure at the end of the bentonite sample

## 5. Testing the influence of the sealing property of bentonite with respect to deep geological repository safety

Although the plug itself does not fulfill a safety function *sensus stricto*, it contributes to the safety function of the bentonite sealing layers by holding the bentonite material in a defined position and ensures that the bentonite remains as much as possible in its predefined form (mainly in terms of bulk density). The requirement for the minimum lifetime of a spent fuel (SF) container is 10 000 years according to the Czech deep geological repository concept. During this time, it is assumed that the SF container will remain undamaged and, therefore, it can be considered as the start time in terms of simulations of deep geological repository (DGR) safety assessments. However, during this time period the bentonite material will



become saturated and may be exposed to the increased inflow of groundwater from structures with increased hydraulic conductivity which, in turn, may affect the structure of the bentonite material surrounding the SF container. It is particularly important to consider the potential formation of erosion channels within the bentonite layer caused by the washing out of the bentonite material. Therefore, the settings of the complex DGR safety assessment using the GoldSim program were changed in order to take into account potential damage suffered by the bentonite layer. The following four bentonite layer variant states were considered (Fig. 36):

1. The bentonite material behind the plug remains intact; no erosion channel has been created
2. An erosion channel has been created within the bentonite material: the channel has been filled with material with a lower bulk density due to the swelling properties of the bentonite material
3. An erosion channel has been created within the bentonite material: the channel has remained empty
4. All the bentonite has been washed out and the space between the plug and the SF canister is empty

With concern to the second and third variants, several erosion channel opening values were simulated. The degree of bentonite layer damage is given by the multiplication of the circumference of the SF container and the percentage of damage (Fig. 37).

From Fig. 37 it is evident that 100% damage in the third variant (empty fissure) corresponds to the fourth variant, namely the state in which the bentonite material has been completely washed out from the space between the borehole wall and the SF canister. It is clear that such a scenario is extremely unlikely and, further, it is necessary to mention that the Czech DGR concept does not consider damage to the bentonite layer to such an extent as does the numerical model. Variants 3 and 4 were simulated so as to highlight the impact of the state of the bentonite layer on the effective dose rate.

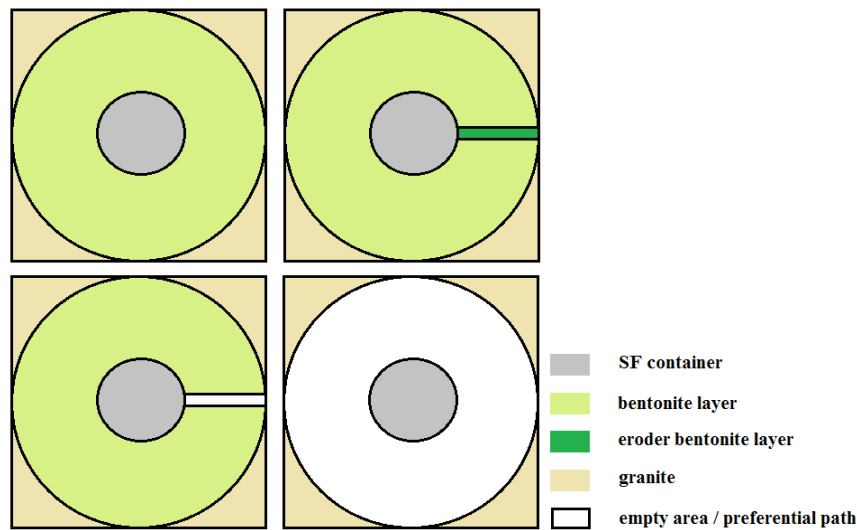


Fig. 36 Four variants considered in the simulation of the bentonite layer.

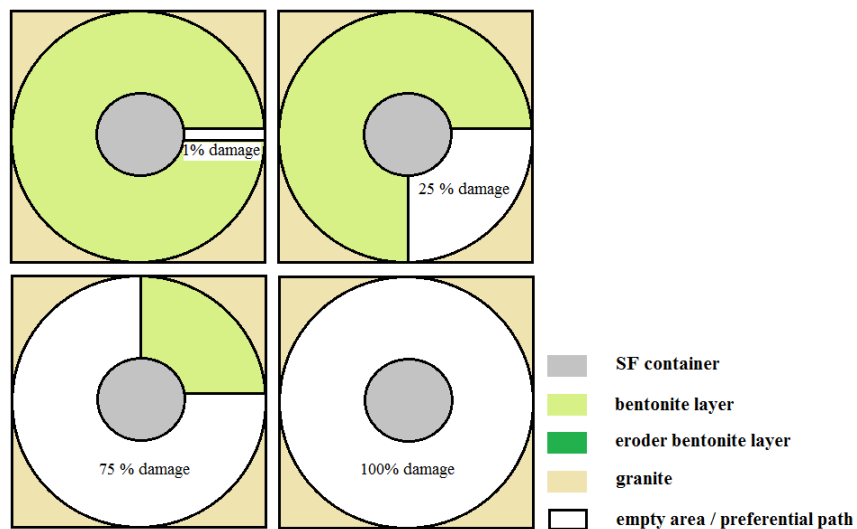


Fig. 37 The rate of damage to the bentonite layer considered in the various simulations.

## 5.1 Conceptual model

The Czech concept concerning the storage of SF and HLW (high-level waste) generally assumes the storage of the waste in SF containers which will be emplaced in boreholes drilled into the rock massif at a depth of around 500m below the earth's surface. The SF containers will be surrounded by a bentonite damping and sealing layer. It is assumed that leakage from the SF containers may occur only following the corrosion of the material of which the SF container is manufactured or following mechanical damage to the SF container. Contamination (activity) may then spread from the SF container through the bentonite damping and sealing layer into the rock environment from which it may be transported via groundwater flow to interfaces with the biosphere.



The model assumes the storage of 6000 SF containers made of carbon steel. The release of activity is assumed to occur following the degradation of the SF container and the transport process is assumed to consist of the diffusion of the water phase inside the SF container into the bentonite layer. The degradation of the SF container is described by a selected distribution curve. The minimum service life of the SF container is set at 10,000 years, and the median is 110,000 years. The degradation of the waste matrix occurs following the degradation of the SF containers from which radionuclides are released into the aqueous phase. The basic rate of degradation of SF (matrix  $UO_x$ ) is  $1e^{-8}$  year<sup>-1</sup> and for activated structural materials  $1e^{-5}$  years<sup>-1</sup>.

The bentonite damping and sealing layer is modelled, for reasons of greater accuracy, by fifteen concentric layers. The outer layer represents the interface with the storage space (the rock environment). The diffusion rock layer is modelled at the bentonite / storage space interface in order to eliminate the influence of advection within the bentonite layer.

The radionuclides are transported by diffusion through the bentonite layer to the storage space (model view only). The storage space is modelled in the form of compartments measuring  $3km \times 1km \times 10m$ . In this area, for each time step, a balance of concentration has been set which means that the same conditions prevail throughout the whole area. Radionuclides from the storage space are transported by the flow of groundwater (advection is considered as the transport process) towards a preferential path in the geosphere.

The geosphere is modelled using “Pipe” components (more than one) that model transport processes such as advection, diffusion into the rock matrix and sorption. Groundwater flows into the compartment which models processes in the biosphere from the final “Pipe”.

The biosphere is modelled by means of four compartments representing land (cultivable and forest), a lake and a river, and represents a universal model that corresponds to the current lifestyle of the Czech Republic. The output of the biosphere model consists of the effective dose rate to humans living in the area affected by underground storage.

## 5.2 Parametric model settings

### A list of considered radionuclides

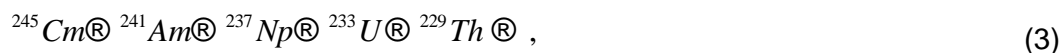
The critical radionuclides considered in the complex model are provided in Tab. 3 which also lists half-life and daughter products, which is important for inventory calculation purposes and the subsequent safety analysis.

Actinides may either reduce the inventory because of their transformation or increase it due to their membership of one of the following conversion rows described in equations (2) and (5)

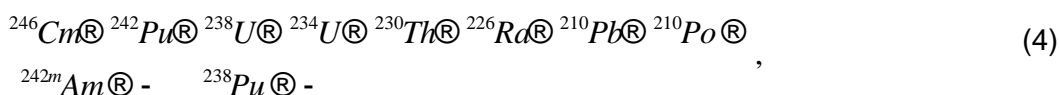
Row  $4n+0$ :



Row  $4n+1$ :



Row  $4n+2$ :



Row 4n+3:



Tab. 3: Half-lives and daughter products. The daughter products have been selected according to the work of Landa (2012) and half-lives according to BIPM [online] and NUDat2.6 [online].

Nuclide	Half-life [years]	Daughter products
Be10	1,51E+06	
C14	5,70E+03	
Cl36	3,01E+05	
Ca41	1,02E+05	
Ni59	7,60E+04	
Ni63	9,87E+01	
Se79	3,56E+05	
Sr90	2,88E+01	
Zr93	1,53E+06	
Nb94	2,03E+04	
Mo93	4,00E+03	
Tc99	2,11E+05	
Pd107	6,50E+06	
Ag108m	4,38E+02	
Sn126	2,30E+05	
I129	1,61E+07	
Cs135	2,30E+06	
Cs137	3,01E+01	
Sm151	9,00E+01	
Ho166m	1,20E+03	
Pb210	2,22E+01	Po210
Po210	3,79E-01	
Ra226	1,60E+03	Pb210



Nuclide	Half-life [years]	Daughter products
Th229	7,88E+03	
Th230	7,54E+04	Ra226
Th232	1,40E+10	
Pa231	3,28E+04	
U233	1,59E+05	Th229
U234	2,46E+05	Th230
U235	7,04E+08	Pa231
U236	2,34E+07	Th232
U238	4,47E+09	U234
Np237	2,14E+06	U233
Pu238	8,77E+01	U234
Pu239	2,41E+04	U235
Pu240	6,56E+03	U236
Pu242	3,73E+05	U238
Am241	4,33E+02	Np237
Am242m	1,41E+02	Pu242
Am243	7,37E+03	Pu239
Cm244	1,81E+01	Pu240
Cm245	8,50E+03	Am241
Cm246	4,72E+03	Pu242

### 5.3 Degradation of the SF container

The Czech deep geological repository concept assumes the storage of seven fuel sets of the VVER 440 type or three sets of the VVER 1000 type in each SF container. It is expected that the SF containers will be made of carbon steel.

The material from which the SF container is made is not considered significant in terms of the mathematical model; from this point of view the distribution curve is significant in terms of the degradation of the SF container. The degradation of SF containers is described by distribution curves obtained by applying the Weibull distribution. When a fault occurs in an SF container, the immediate release occurs of part of the inventory (IRF – the instant release fraction), and from this point onwards the waste matrix suffers degradation, i.e. UO<sub>2</sub>, MO<sub>x</sub>, construction materials and cement matrix.



The release rate of radionuclides from the waste matrix is directly proportional to the degradation rate of the matrix. The process is described by equation (6); the degradation rate of the waste matrix is listed in Tab. 4.

$$\frac{dm_{mat,j}}{dt} = k_{mat} \times m_{mat,j}, \quad (6)$$

where

$\frac{dm_{mat,j}}{dt}$  the release rate of radionuclide  $j$  from matrix, [M.T<sup>-1</sup>],

$k_{mat}$  the relative decrease of the matrix [T<sup>-1</sup>],

$m_{mat,j}$  amount of a radionuclide in the matrix [M].

Tab. 4: Degradation rate of the waste matrix according to Vokál et al. (2010).

Matrix	Degradation rate [year <sup>-1</sup> ]
UOx	1E-08
MOx	1E-08
construction materials	1E-05
vitified matrix	1E-07
cement matrix	1E-03

#### 5.4 Bentonite damping and sealing layer

A bentonite layer surrounds each SF container which performs a damping and sealing function. The thickness of this layer is around 0.7m. The bentonite barrier is divided into fifteen concentric layers in the mathematical model (Fig. 38). The transport of radionuclides through the bentonite layer occurs solely by means of diffusion.

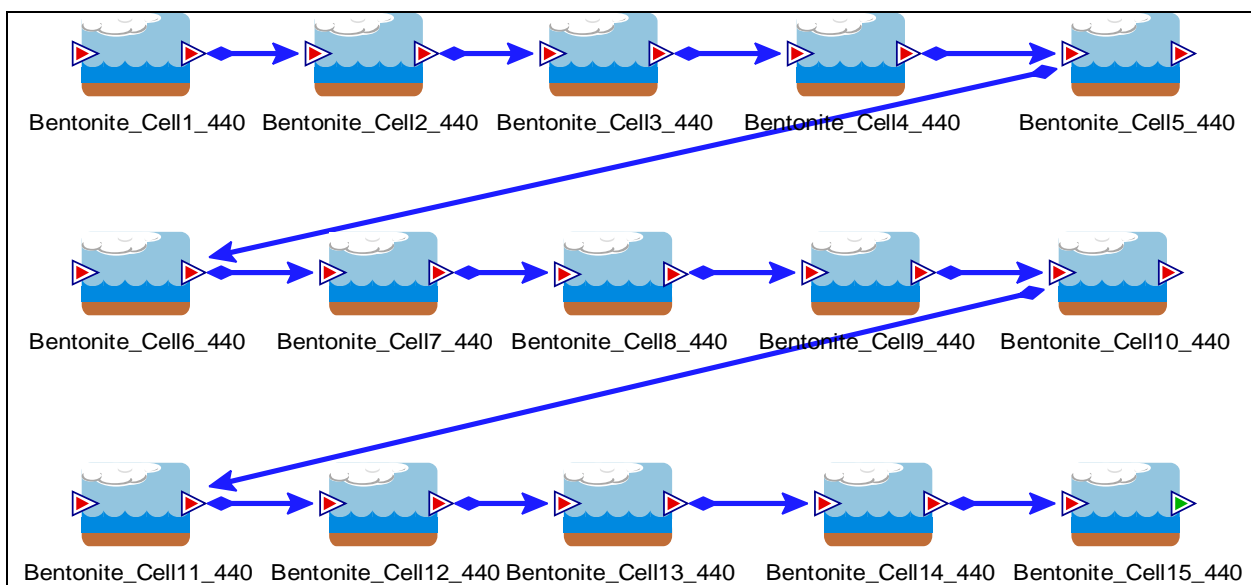


Fig. 38 Schematic model of the bentonite barrier.

The following parameters are important for the modelling of a given element within the bentonite material (Tab. 5):

- Solubility limit of the element
- Distribution coefficient  $K_d$  of the element
- The diffusion coefficient  $D_e$
- Diffusion coefficient of a species in water  $D_{w,25}$

Tab. 5 Transport parameters of the bentonite layers used in the complex model. A value of -1 indicates unlimited solubility.

Nuclide	Solubility [mol.dm <sup>-3</sup> ]	$D_e$ [m <sup>2</sup> /s]	$D_w$ [m <sup>2</sup> /s]	$K_d$ [m <sup>3</sup> /kg]
Be10	-1,00E+00	2,00E-10	5,99E-10	2,00E-01
C14	-1,00E+00	1,20E-10	9,23E-10	0,00E+00
Cl36	-1,00E+00	1,00E-11	2,03E-09	0,00E+00
Ca41	1,00E-02	2,00E-10	7,92E-10	3,00E-03
Mn54	0,00E+00	5,11E-11	5,11E-10	0,00E+00
Co60	0,00E+00	5,11E-11	5,11E-10	0,00E+00
Ni59	8,00E-05	1,20E-10	6,61E-10	7,00E-02
Ni63	8,00E-05	1,20E-10	6,61E-10	7,00E-02
Se79	1,00E-05	1,00E-11	9,59E-10	0,00E+00
Sr90	1,00E-04	1,20E-10	7,91E-10	1,00E-03
Zr93	2,00E-09	1,20E-10	5,00E-10	5,00E+00



Nuclide	Solubility [mol.dm <sup>-3</sup> ]	De [m <sup>2</sup> /s]	Dw [m <sup>2</sup> /s]	Kd [m <sup>3</sup> /kg]
Nb94	1,00E-04	1,20E-10	5,00E-10	3,00E+00
Mo93	1,00E-05	3,00E-12	1,98E-09	0,00E+00
Tc99	1,00E-08	1,20E-10	1,50E-09	4,00E+01
Pd107	2,00E-07	1,20E-10	7,19E-10	5,00E+00
Ag108m	3,00E-06	1,20E-10	1,65E-09	0,00E+00
Sn126	1,00E-07	1,20E-10	5,00E-10	4,00E+01
I129	-1,00E+00	1,00E-11	2,05E-09	0,00E+00
Cs135	-1,00E+00	3,00E-10	2,07E-09	3,00E-02
Cs137	-1,00E+00	3,00E-10	2,07E-09	3,00E-02
Sm151	9,00E-07	1,20E-10	6,08E-10	5,00E+00
Eu152	0,00E+00	5,11E-11	5,11E-10	0,00E+00
Ho166m	9,00E-07	1,20E-10	5,89E-10	5,00E+00
Pb210	8,00E-05	2,00E-10	9,30E-10	5,50E-01
Po210	-1,00E+00	3,00E-12	5,00E-10	3,00E+00
Ra226	5,00E-08	1,20E-10	8,89E-10	1,00E-03
Th229	3,00E-06	1,20E-10	5,00E-10	4,00E+01
Th230	3,00E-06	1,20E-10	5,00E-10	4,00E+01
Th232	3,00E-06	1,20E-10	5,00E-10	4,00E+01
Pa231	1,00E-05	1,20E-10	5,00E-10	3,00E+00
U233	5,00E-07	1,20E-10	4,26E-10	1,00E+01
U234	5,00E-07	1,20E-10	4,26E-10	1,00E+01
U235	5,00E-07	1,20E-10	4,26E-10	1,00E+01
U236	5,00E-07	1,20E-10	4,26E-10	1,00E+01
U238	5,00E-07	1,20E-10	4,26E-10	1,00E+01
Np237	1,00E-08	1,20E-10	5,00E-10	4,00E+01
Pu238	1,00E-06	1,20E-10	5,70E-10	4,00E+01
Pu239	1,00E-06	1,20E-10	5,70E-10	4,00E+01
Pu240	1,00E-06	1,20E-10	5,70E-10	4,00E+01
Pu242	1,00E-06	1,20E-10	5,70E-10	4,00E+01



Nuclide	Solubility [mol.dm <sup>-3</sup> ]	De [m <sup>2</sup> /s]	Dw [m <sup>2</sup> /s]	Kd [m <sup>3</sup> /kg]
Am241	3,00E-05	1,20E-10	6,02E-10	2,40E+01
Am242m	3,00E-05	1,20E-10	6,02E-10	2,40E+01
Am243	3,00E-05	1,20E-10	6,02E-10	2,40E+01
Cm244	3,00E-05	1,20E-10	5,97E-10	2,40E+01
Cm245	3,00E-05	1,20E-10	5,97E-10	2,40E+01
Cm246	3,00E-05	1,20E-10	5,97E-10	2,40E+01

## 5.5 Simulation of an erosion channel

An erosion channel was simulated using the “Pipe” component in versions 2 and 3 wherein the erosion channel in variant 2 has mineral fillings and in variant 3 it is empty. In the case of both versions 2 and 3, the volume of intact bentonite decreases with the increasing radius of the erosion channel. Intact bentonite was completely omitted in version 4 - the released radionuclides are transported through a “Pipe” component directly into the storage space following damage to the SF container.

It is clear that extreme damage to the bentonite layer is completely unrealistic primarily because of the structure of the mathematical model. The Czech concept based on SF containers assumes that all the containers will eventually be damaged; container damage over time is controlled by the Weibull distribution. The SF container together with the surrounding bentonite layer is simulated as a whole in the mathematical model; not all the 6000 containers are present, rather one container is multiplied by 6000. It was therefore not possible to simulate damage to the bentonite layer only around one SF container; the mathematical model assumes damage to all 6,000 damping and sealing layers.

A change to the parameters of the mineral filling in version 3 was made in the following manner:

- Decrease in the density of 50%,
- Increase in the porosity of 50%
- Decrease in  $K_d$  by 50%,
- Increase in  $D_e$  by 50%.

It was assumed that with decreasing density, the porosity of the material would increase due to the increase in free pore volume while maintaining the volume of the material. Furthermore, an increase in  $D_e$  was assumed again due to an increase in free pore volume in which the diffusion of radionuclides might occur. Finally, a decrease in  $K_d$  was considered due to a decrease in the amount of material and thus the loss of sorption sites.

## 5.6 Geosphere

The Geosphere model is composed of three “Pipe” components and the principal characteristics of the transport routes are (Fig. 39):



- Flow rate of groundwater from the storage space to the preferential path
- Time of groundwater flow from the storage space to the geosphere/biosphere interface,
- The flow rate of groundwater,
- The ratio of the inflow and runoff of individual “Pipe” components

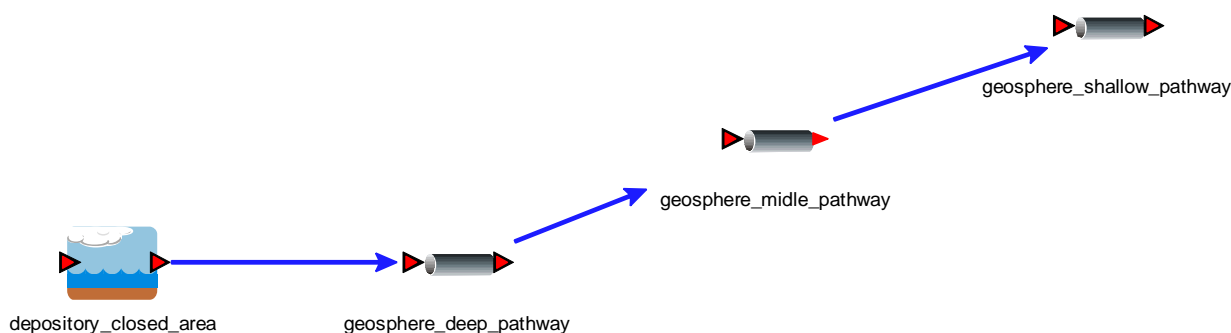


Fig. 39 Geosphere model using “Pipe” components.

The following parameters are important in terms of the modelling of a given element in the geosphere (Tab. 6):

- Wetted surface ( $a_{wi}$ ), a reference value of 0.1 was used.
- The porosity of the rock matrix ( $\theta_m$ ), a reference value of 0.5 was used.
- The diffusion coefficients of the rock matrix ( $D_e$  a  $D_w$ ),
- Sorption coefficients for radionuclides in the rock matrix and the fracture infill materials ( $K_d$ ),
- The solubility limit of the element

Tab. 6 Transport parameters of the granite layers used in the complex model. A value of -1 indicates unlimited solubility.

Nuclide	Solubility [mol.dm <sup>-3</sup> ]	De [m <sup>2</sup> /s]	Dw [m <sup>2</sup> /s]	Kd [m <sup>3</sup> /kg]
Be10	1,00E-08	2,40E-14	5,99E-10	1,00E-01
C14	-1,00E+00	5,00E-15	9,23E-10	5,00E-04
Cl36	-1,00E+00	8,00E-15	2,03E-09	0,00E+00
Ca41	-1,00E+00	5,00E-14	7,92E-10	1,00E-04
Mn54	5,60E-05	5,11E-13	5,11E-10	0,00E+00
Co60	-1,00E+00	5,11E-13	5,11E-10	0,00E+00



Nuclide	Solubility [mol.dm <sup>-3</sup> ]	De [m <sup>2</sup> /s]	Dw [m <sup>2</sup> /s]	Kd [m <sup>3</sup> /kg]
Ni59	-1,00E+00	2,80E-14	6,61E-10	1,00E-02
Ni63	-1,00E+00	2,80E-14	6,61E-10	1,00E-02
Se79	2,59E-06	4,00E-14	9,59E-10	5,00E-04
Sr90	1,21E-01	3,00E-13	7,91E-10	1,00E-04
Zr93	2,51E-06	4,00E-14	5,00E-10	5,00E-01
Nb94	1,27E-05	4,00E-14	5,00E-10	5,00E-01
Mo93	1,00E-03	1,00E-15	1,98E-09	5,00E-04
Tc99	7,90E-06	4,00E-14	1,50E-09	3,00E-01
Pd107	4,20E-07	4,00E-14	7,19E-10	1,00E-03
Ag108m	7,20E-04	4,00E-14	1,65E-09	1,00E-01
Sn126	4,70E-06	4,00E-14	5,00E-10	0,00E+00
I129	-1,00E+00	8,00E-15	2,05E-09	0,00E+00
Cs135	-1,00E+00	9,00E-13	2,07E-09	1,00E-02
Cs137	-1,00E+00	9,00E-13	2,07E-09	1,00E-02
Sm151	8,03E-04	4,00E-14	6,08E-10	1,00E+00
Eu152	2,00E-03	5,11E-13	5,11E-10	0,00E+00
Ho166m	7,12E-04	4,00E-14	5,89E-10	1,00E+00
Pb210	8,00E-02	4,00E-14	9,30E-10	2,70E-01
Po210	-1,00E+00	4,00E-14	5,00E-10	1,50E-01
Ra226	1,20E-01	3,70E-14	8,89E-10	1,00E-02
Th229	1,22E-06	6,30E-15	5,00E-10	1,00E+00
Th230	1,22E-06	6,30E-15	5,00E-10	1,00E+00
Th232	1,22E-06	6,30E-15	5,00E-10	1,00E+00
Pa231	3,20E-04	4,00E-14	5,00E-10	5,00E-01
U233	1,29E-04	4,00E-14	4,26E-10	1,00E+00
U234	1,29E-04	4,00E-14	4,26E-10	1,00E+00
U235	1,29E-04	4,00E-14	4,26E-10	1,00E+00
U236	1,29E-04	4,00E-14	4,26E-10	1,00E+00
U238	1,29E-04	4,00E-14	4,26E-10	1,00E+00



Nuclide	Solubility [mol.dm <sup>-3</sup> ]	De [m <sup>2</sup> /s]	Dw [m <sup>2</sup> /s]	Kd [m <sup>3</sup> /kg]
Np237	5,90E-05	4,00E-14	5,00E-10	1,00E+00
Pu238	1,38E-07	4,00E-14	5,70E-10	1,00E+00
Pu239	1,38E-07	4,00E-14	5,70E-10	1,00E+00
Pu240	1,38E-07	4,00E-14	5,70E-10	1,00E+00
Pu242	1,38E-07	4,00E-14	5,70E-10	1,00E+00
Am241	9,40E-05	4,00E-14	6,02E-10	1,00E+00
Am242m	9,40E-05	4,00E-14	6,02E-10	1,00E+00
Am243	9,40E-05	4,00E-14	6,02E-10	1,00E+00
Cm244	9,01E-06	4,00E-14	5,97E-10	1,00E+00
Cm245	9,01E-06	4,00E-14	5,97E-10	1,00E+00
Cm246	9,01E-06	4,00E-14	5,97E-10	1,00E+00

## 5.7 Biosphere

The biosphere model is designed so that contaminated water from the geosphere flows into agricultural areas, farmland, forest land and lakes. Vegetable crops are cultivated and livestock is kept in this area. People living in this area consume only the products of local farming and do not import food and beverages from elsewhere.

The following contamination paths are considered in the model with respect to the biosphere (Fig. 40):

- Ingestion
  - water,
  - plant products, root vegetables, leafy vegetables including the re-suspension of dust, potatoes and mushrooms,
  - soil.
- Dust inhalation (soil)
- External beam radiation
  - From the air (dust),
  - from soil,
  - from water.

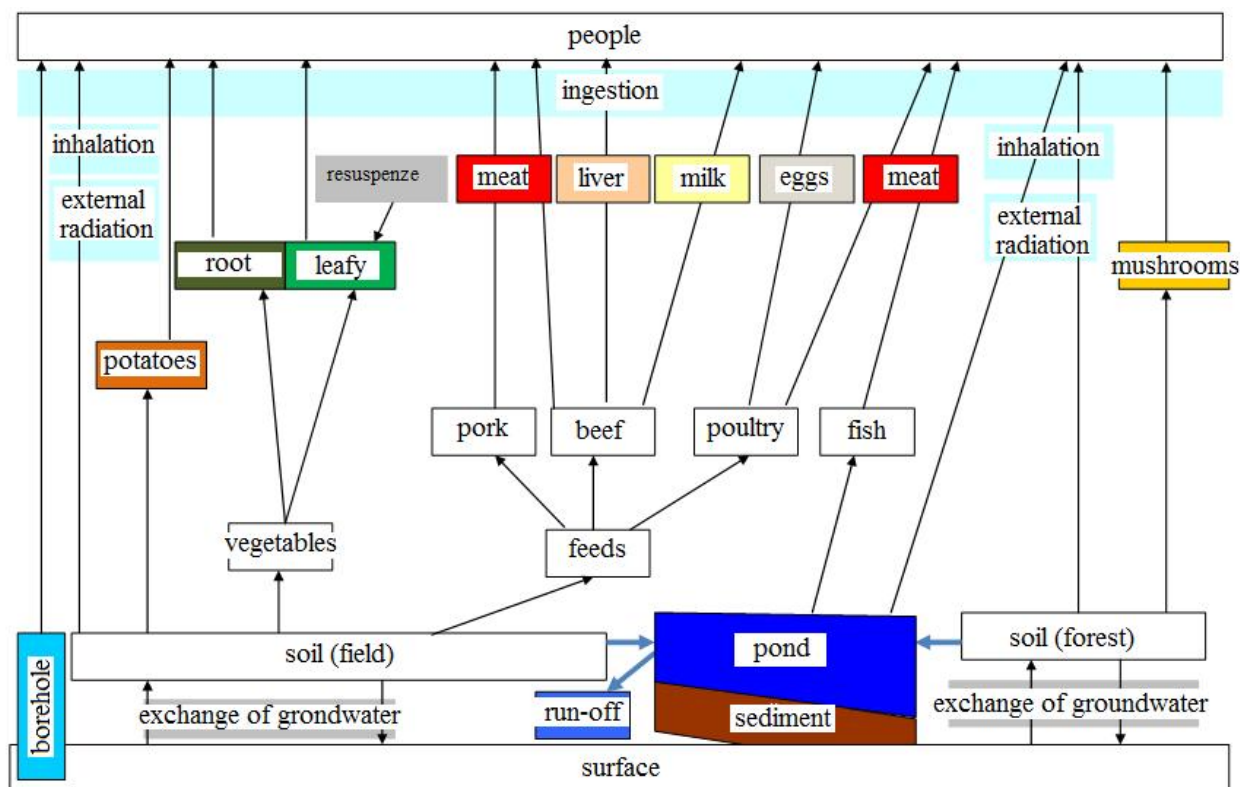


Fig. 40 Extended conceptual model of the biosphere (Trpkošová, 2013).

The following parameters are important in terms of the modelling of a given element in the biosphere:

- Transfer factors for plants (Tab. 7),
- Transfer factors for animal products (Tab. 8),
- Hydrological data (Tab. 9),
- Baskets for the biosphere models (Tab. 10),
- Batch conversion factors (Tab. 11).

Tab. 7: Transfer factors for plants [-], by the IAEA (2010) and Staven et al. (2003).

Element	Root vegetables	Leafy vegetables	Feed	Potatoes	Mushrooms
Be	0,01	1,00E-02	0,42	0,01	0,01
C	0,7	0,7	0,7	0,7	5,5
Cl	12	70	30	70	300
Ca	0,35	3,5	3,5	0,35	0,875
Ni	0,062	0,28	0,2	0,3	0,52
Se	0,05	0,25	20	0,05	0,6
Sr	0,5	1,2	1	1,6	1,4



Element	Root vegetables	Leafy vegetables	Feed	Potatoes	Mushrooms
Zr	0,004	0,004	0,04	0,002	0,002
Nb	0,017	0,017	0,02	0,004	0,01
Mo	0,32	0,51	0,8	0,8	0,8
Tc	46	250	76	0,18	78
Pd	0,04	0,15	0,2	0,04	0,15
Ag	0,0013	0,00018	0,00018	0,0013	0,0039
Sn	0,006	0,03	0,1	0,006	0,03
I	0,04	0,04	0,6	0,04	0,034
Cs	0,042	0,074	0,25	0,14	10,2
Sm	0,02	0,02	0,01	0,02	0,02
Ho	0,02	0,02	0,001	0,02	0,02
Pb	0,015	0,82	0,092	0,015	1
Po	0,077	0,0074	0,12	0,077	0,077
Ra	0,07	0,12	0,071	0,12	0,12
Th	0,0008	0,00086	0,0087	0,0036	0,21
Pa	0,00035	0,00047	3	0,00035	0,00035
U	0,0084	0,043	0,046	0,08	0,08
Np	0,022	0,027	0,061	0,027	0,027
Pu	0,00039	0,00028	0,00055	0,005	0,005
Am	0,00067	0,00016	0,0015	0,0047	0,0047
Cm	0,00085	0,0014	0,001	0,0021	0,0021

Tab. 8: Transfer factors for animal products by the IAEA (2010) and Staven et al. (2003).

Element	Beef [d·kg-1]	Milk [d·l-1]	Liver [d·kg-1]	Pork [d·kg-1]	Poultry meat [d·kg-1]	Eggs [d·kg-1]	Fish [l·kg-1]
Be	0,001	8,3E-07	0,01	0,001	4,00E-01	2,00E-02	1,00E+02
C	0,031	0,012	0,1	0,031	0,031	0,031	3,20E+05
Cl	0,017	0,017	0,02	0,02	3,00E-02	2,70E+00	2,30E+02
Ca	0,013	0,01	0,61	2,00E-03	4,40E-02	4,40E-01	5,60E+03
Ni	0,005	0,00095	0,05	2,00E-01	1,00E-03	1,00E-01	6,60E+02
Se	0,015	0,004	10	3,20E-01	9,7	1,60E+01	1,20E+04



Element	Beef [d·kg-1]	Milk [d·l-1]	Liver [d·kg-1]	Pork [d·kg-1]	Poultry meat [d·kg-1]	Eggs [d·kg-1]	Fish [l·kg-1]
Sr	0,0013	0,0013	0,01	2,50E-03	2,00E-02	3,50E-01	7,10E+02
Zr	1,2E-06	3,6E-06	0,01	0,000001	6,00E-05	2,00E-04	2,40E+02
Nb	2,6E-07	4,1E-07	0,01	3E-07	3,00E-04	1,00E-03	3,00E+02
Mo	0,001	0,0011	0,02	0,001	1,80E-01	6,40E-01	1,90E+02
Tc	0,0001	0,00014	0,00075	0,0001	3,00E-02	3,00E+00	2,00E+01
Pd	0,004	0,01	0,01	0,004	3,00E-04	4,00E-03	1,00E+01
Ag	0,003	0,00005	0,006	0,003	2,00E+00	5,00E-01	2,10E+02
Sn	0,08	0,001	0,03	0,08	8,00E-01	1,00E+00	3,00E+03
I	0,0067	0,0054	0,004	4,10E-02	8,70E-03	2,4	4,50E+04
Cs	0,022	0,0046	0,096	0,05	2,7	4,00E-01	2,40E+04
Sm	0,00002	0,00003	0,05	0,00002	2,00E-03	4,00E-05	3,00E+01
Ho	0,00002	0,00003	0,05	0,00002	2,00E-03	4,00E-05	3,00E+01
Pb	0,0007	0,00019	0,0007	0,0004	8,00E-01	3,1	5,70E+03
Po	0,005	0,00021	0,005	0,005	2,4	1,00E+00	1,70E+02
Ra	0,0017	0,00038	0,01	0,0009	3,00E-02	3,10E-01	2,50E+02
Th	0,00023	0,000005	0,00006	0,00004	6,00E-03	4,00E-03	3,90E+03
Pa	0,00004	0,000005	0,0001	0,00004	6,00E-03	4,00E-03	10
U	0,00039	0,0018	0,00063	4,40E-02	7,50E-01	1,1	2,00E+01
Np	2,6E-07	0,000005	0,01	0,001	6,00E-03	4,00E-03	3,00E+01
Pu	1,1E-06	1,1E-06	0,0003	0,00001	3,00E-03	1,20E-03	5,00E+04
Am	0,0005	4,2E-07	0,0001	0,00004	6,00E-03	3,00E-03	4,00E+02
Cm	0,00004	0,00002	0,0002	0,00004	6,00E-03	4,00E-03	3,00E+01

Tab. 9: Hydrological data.

Parameter	Unit	Value	Source
Base flow	l·s-1·km-2	2	Krásný et al. (1982)
The area of cultivated land	ha	100	estimate
The thickness of cultivated land	m	0,3	estimate
Dustiness	m <sup>3</sup> ·kg-1	5,E-06	Fiedler et al. (2004)



Parameter	Unit	Value	Source
Soil moisture		70	estimate
Proportion fields	%	57,67	WZČ [online] ISSaR [online]
The volume of the lake	m <sup>3</sup>	3E+06	estimate according to Janda et al. (1996)
The area of the lake	m <sup>2</sup>	1,74E+06	estimate according to Janda et al. (1996)
The thickness of the bottom sediments	m	0.2	estimate
Resuspension factor	d·m <sup>-1</sup>	1,2E-06	IAEA (2012)
Yield leafy vegetables	kg·m <sup>-2</sup>	2,7	Biozahrada [online] Fialová [online]
Vegetation period of leafy vegetables	month	3	estimate

Tab. 10: Baskets for the biosphere models. Source values were from ČSÚ (2008) SZÚ (2008) publications and Komárek et al. (2008). Unit “a” denotes the year.

Path	Units	Consumption	
Vegetables	Root	kg·a <sup>-1</sup>	27,7
	Leafy	kg·a <sup>-1</sup>	50,1
Potatoes		kg·a <sup>-1</sup>	99,2
Mushrooms		kg·a <sup>-1</sup>	1,9
Meat	Beef	kg·a <sup>-1</sup>	21,0
	Pork	kg·a <sup>-1</sup>	37,8
	Poultry meat	kg·a <sup>-1</sup>	13,5
Milk		l·a <sup>-1</sup>	215,4
Liver		kg·a <sup>-1</sup>	4,4
Eggs		kg·a <sup>-1</sup>	15,4
Fish		kg·a <sup>-1</sup>	5,2
Soil		kg·a <sup>-1</sup>	0,0183
Water		m <sup>3</sup> ·a <sup>-1</sup>	1



Path	Units	Consumption
Respiration rate	m <sup>3</sup> ·a <sup>-1</sup>	8500
Food total	kg·a <sup>-1</sup>	492

Tab. 11: Batch conversion factors. Source values from Vyhl. 307/2002 Sb. publications

Nuclide	h_ing [Sv·Bq <sup>-1</sup> ]	h_inh [Sv·Bq <sup>-1</sup> ]	h_ext_soil [(Sv·s <sup>-1</sup> )/(Bq <sup>-1</sup> ·m <sup>-3</sup> )]	h_ext_air [(Sv·s <sup>-1</sup> )/(Bq <sup>-1</sup> ·m <sup>-3</sup> )]	h_ext_water [(Sv·s <sup>-1</sup> )/(Bq <sup>-1</sup> ·m <sup>-3</sup> )]
Be10	1,10E-09	3,50E-08	5,76E-21	1,12E-17	2,17E-20
C14	5,80E-10	5,80E-09	7,20E-23	2,24E-19	4,39E-22
Cl36	9,30E-10	7,30E-09	1,28E-20	2,23E-17	4,48E-20
Ca41	1,90E-10	1,80E-10	0	0	0
Ni59	6,30E-11	4,40E-10	0	0	0
Ni63	1,50E-10	1,30E-09	0	0	0
Se79	2,90E-09	6,80E-09	9,96E-23	3,03E-19	5,93E-22
Sr90	2,80E-08	1,60E-07	3,77E-21	7,53E-18	1,46E-20
Zr93	1,10E-09	2,50E-08	0	0	0
Nb94	1,70E-09	4,90E-08	5,18E-17	7,70E-14	1,67E-16
Mo93	3,10E-09	2,30E-09	3,16E-21	2,52E-17	5,92E-20
Tc99	6,40E-10	1,30E-08	6,72E-22	1,62E-18	3,14E-21
Pd107	3,70E-11	5,90E-10	0	0	0
Ag108m	2,30E-09	3,70E-08	5,16E-17	7,80E-14	1,69E-16
Sn126	4,70E-09	2,80E-08	7,89E-19	2,11E-15	4,76E-18
I129	1,10E-07	3,60E-08	6,93E-20	3,80E-16	8,91E-19
Cs135	2,00E-09	8,60E-09	2,05E-22	5,65E-19	1,10E-21
Cs137	1,30E-08	3,90E-08	4,02E-21	7,74E-18	1,49E-20
Sm151	9,80E-11	4,00E-09	5,27E-24	3,61E-20	8,50E-23
Ho166m	2,00E-09	1,20E-07	5,51E-17	8,45E-14	1,84E-16
Pb210	6,90E-07	5,60E-06	1,31E-20	5,64E-17	1,31E-19
Po210	1,20E-06	4,30E-06	2,80E-22	4,16E-19	9,03E-22
Ra226	2,80E-07	9,50E-06	1,70E-19	3,15E-16	6,95E-19



Nuclide	$h_{ing}$ [Sv·Bq <sup>-1</sup> ]	$h_{inh}$ [Sv·Bq <sup>-1</sup> ]	$h_{ext\_soil}$ [(Sv·s <sup>-1</sup> )/(Bq <sup>-1</sup> ·m <sup>-3</sup> )]	$h_{ext\_air}$ [(Sv·s <sup>-1</sup> )/(Bq <sup>-1</sup> ·m <sup>-3</sup> )]	$h_{ext\_water}$ [(Sv·s <sup>-1</sup> )/(Bq <sup>-1</sup> ·m <sup>-3</sup> )]
Th229	4,90E-07	2,40E-04	1,72E-18	3,83E-15	8,56E-18
Th230	2,10E-07	1,00E-04	6,47E-21	1,74E-17	3,94E-20
Th232	2,30E-07	1,10E-04	2,79E-21	8,72E-18	1,99E-20
Pa231	7,10E-07	1,40E-04	1,02E-18	1,72E-15	3,78E-18
U233	5,10E-08	9,60E-06	7,48E-21	1,63E-17	3,64E-20
U234	4,90E-08	9,40E-06	2,15E-21	7,63E-18	1,75E-20
U235	4,70E-08	8,50E-06	3,86E-18	7,20E-15	1,59E-17
U236	4,70E-08	8,70E-06	1,15E-21	5,01E-18	1,16E-20
U238	4,50E-08	8,00E-06	5,52E-22	3,41E-18	7,95E-21
Np237	1,10E-07	5,00E-05	4,17E-19	1,03E-15	2,32E-18
Pu238	2,30E-07	1,10E-04	8,10E-22	4,88E-18	1,14E-20
Pu239	2,50E-07	1,20E-04	1,58E-21	4,24E-18	9,60E-21
Pu240	2,50E-07	1,20E-04	7,85E-22	4,75E-18	1,11E-20
Pu242	2,40E-07	1,10E-04	6,85E-22	4,01E-18	9,35E-21
Am241	2,00E-07	9,60E-05	2,34E-19	8,18E-16	1,88E-18
Am242m	1,90E-07	9,20E-05	9,04E-21	3,17E-17	7,28E-20
Am243	2,00E-07	9,60E-05	7,60E-19	2,18E-15	4,94E-18
Cm244	1,20E-07	5,70E-05	6,74E-22	4,91E-18	1,15E-20
Cm245	2,10E-07	9,90E-05	1,82E-18	3,96E-15	8,84E-18
Cm246	2,10E-07	9,80E-05	6,22E-22	4,46E-18	1,05E-20

## 6. Results and discussion

The development of the effective dose rate in the case of the empty piping channel (variant 3) with respect to various degrees of damage of the bentonite layer is shown in Fig. 41, and that of the filled piping channel (option 2) in Fig. 42. A comparison of the development of the effective dose rate for the same level of violations with regard to different tasks (for both the empty and filled piping channels) is shown in Fig. 43 - Fig. 49. The contributions of individual radionuclides to the total effective dose rate concerning the empty and filled piping channels for differing degrees of damage is shown in Fig. 50 - Fig. 54.

The graphs in Fig. 41 and Fig. 42 reveal that the effective dose rate grows with an increase in the rate of damage to the bentonite layer. The explanation for this phenomenon consists of the loss of material available for the sorption of radionuclides. In the case of a decrease in



sorption sites, a greater number of radionuclides access the water (their concentration in the water increases).

The significant influence of the effective dose rate can be seen in the case of the empty piping channel with a degree of damage of 99% and a 99.99% contribution of  $^{126}\text{Sn}$ . The contribution of  $^{126}\text{Sn}$  is also evident in the case of the filled piping channel, although different trends are exhibited over time.

In terms of problems concerning the empty piping channel, the contribution of  $^{126}\text{Sn}$ ,  $^{229}\text{Th}$ ,  $^{230}\text{Th}$  and  $^{242}\text{Pu}$  radionuclides to the total effective dose increases with the degree of damage to the bentonite layers.

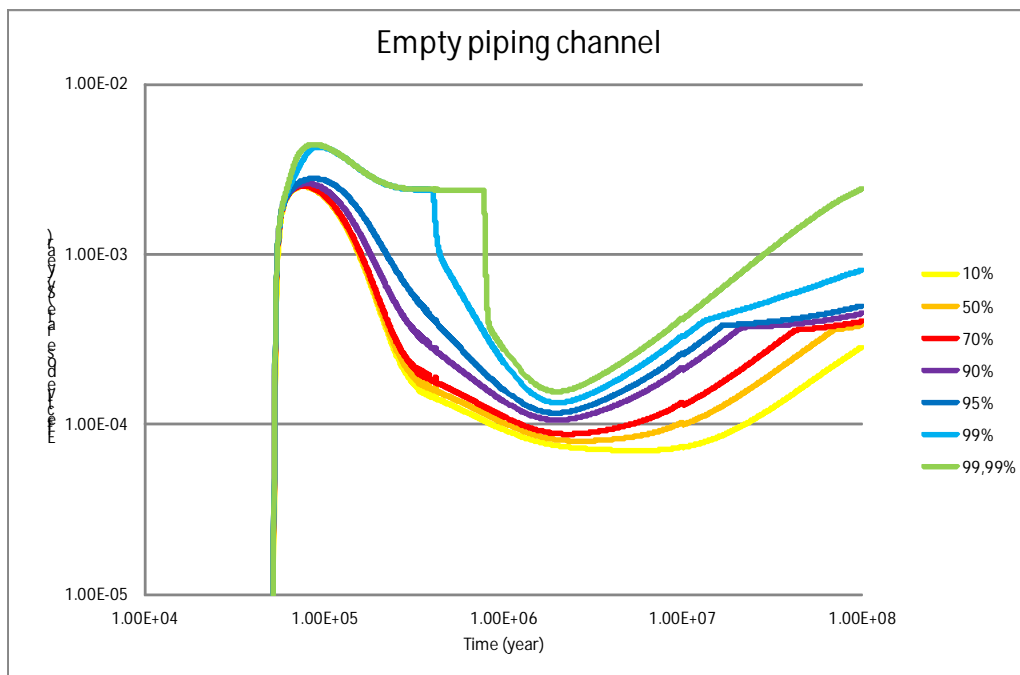


Fig. 41 Development of the effective dose rate in the case of the empty piping channel for different degrees of damage to the bentonite layer.

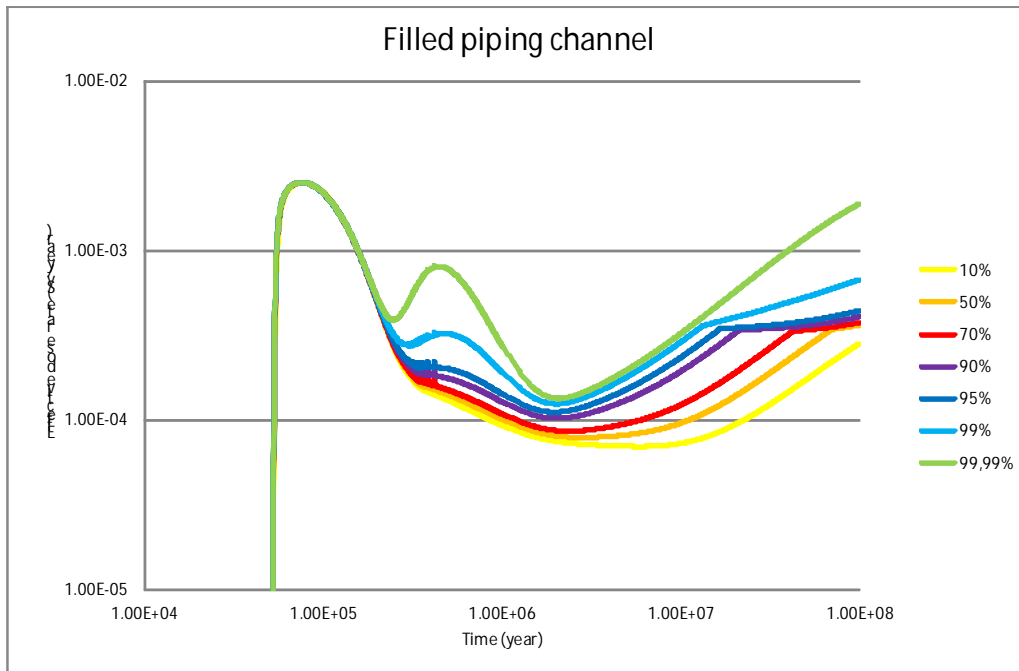


Fig. 42 Development of the effective dose rate in the case of the filled piping channel for different degrees of damage to the bentonite layer.

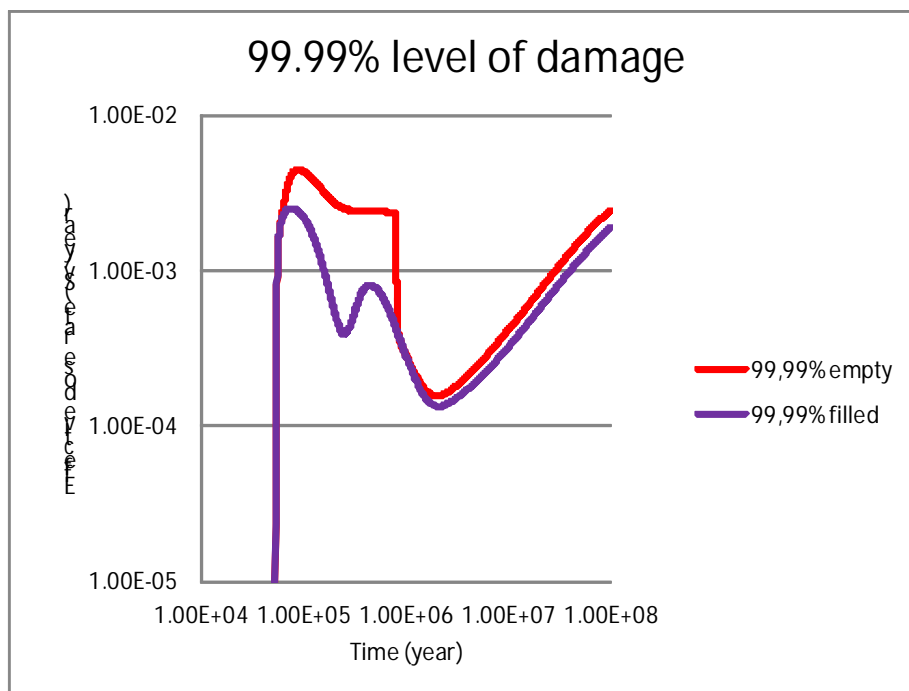


Fig. 43 Comparison of the development of the effective dose rate with concern to the empty and filled erosion channels with 99.99% damage to the bentonite layer. The case of the empty erosion channel corresponds to a situation in which the bentonite was completely washed out.

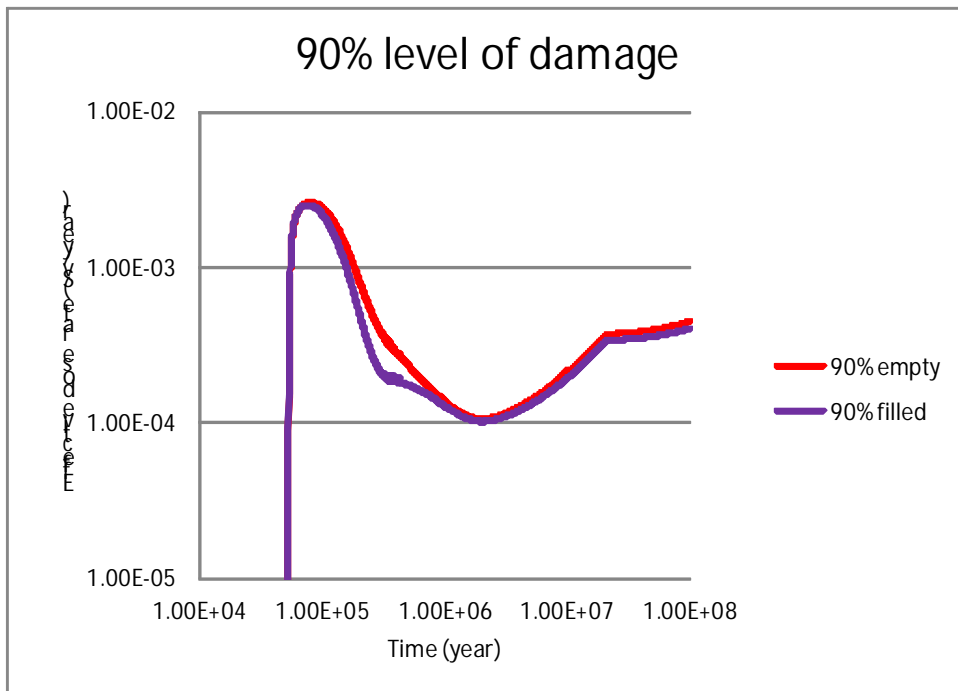


Fig. 44 Comparison of the development of the effective dose rate with concern to the empty and filled erosion channels with 99% damage to the bentonite layer.

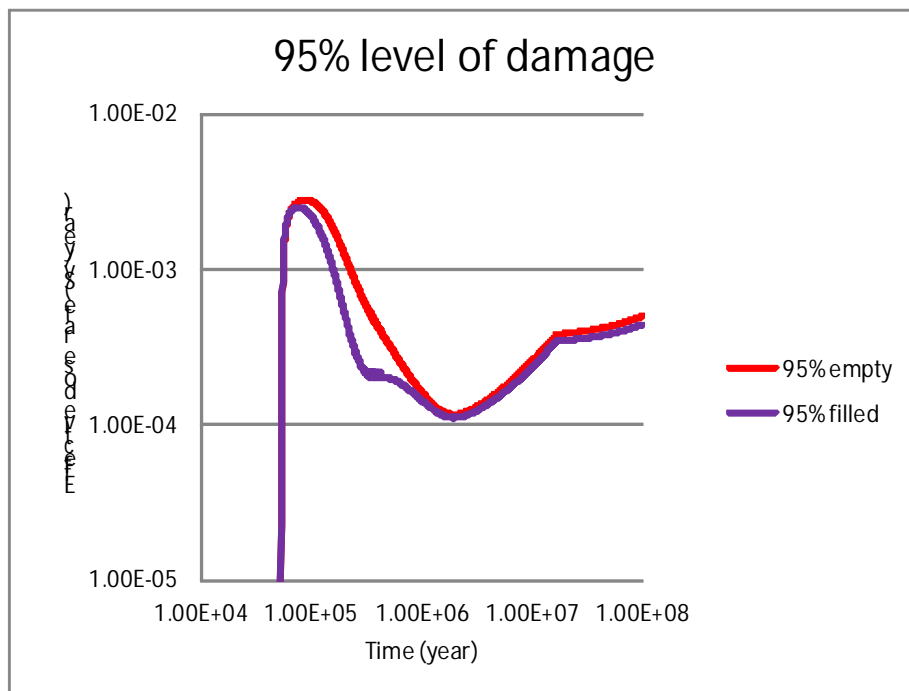


Fig. 45 Comparison of the development of the effective dose rate with concern to the empty and filled erosion channels with 95% damage to the bentonite layer.

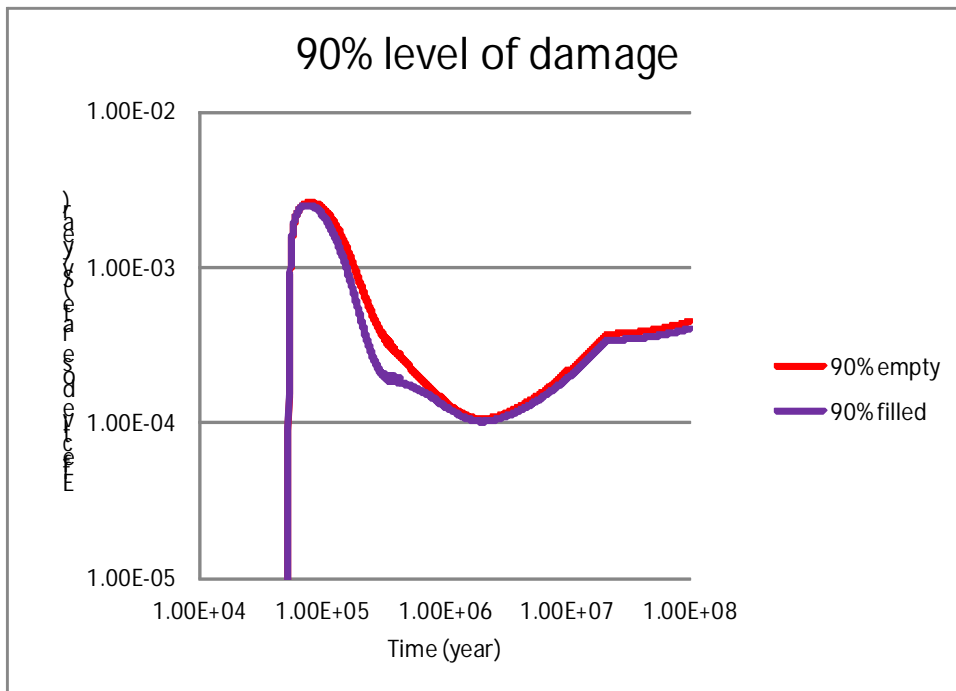


Fig. 46 Comparison of the development of the effective dose rate with concern to the empty and filled erosion channels with 90% damage to the bentonite layer.

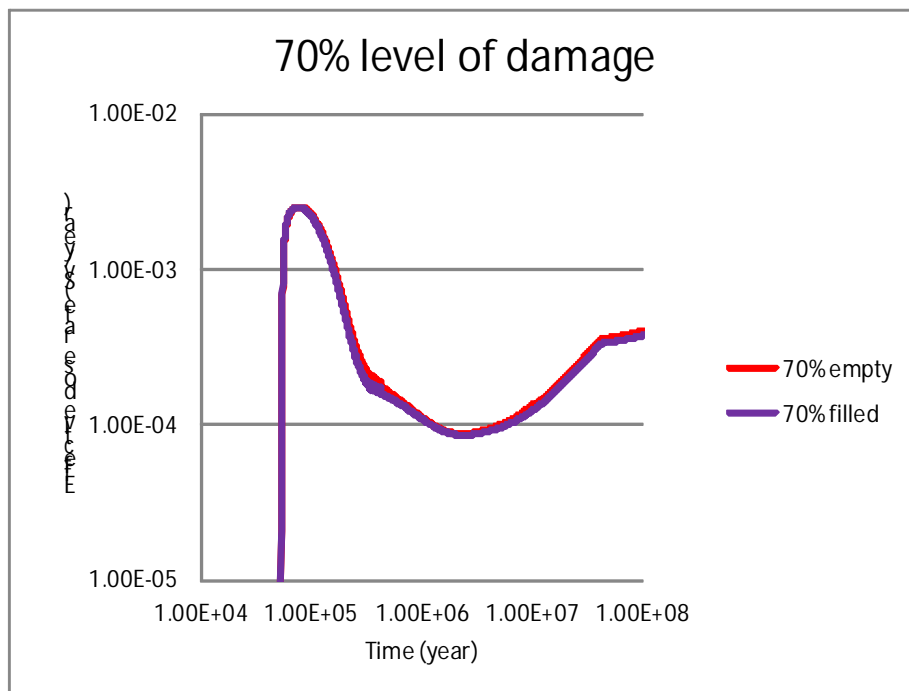


Fig. 47 Comparison of the development of the effective dose rate with concern to the empty and filled erosion channels with 70% damage to the bentonite layer.

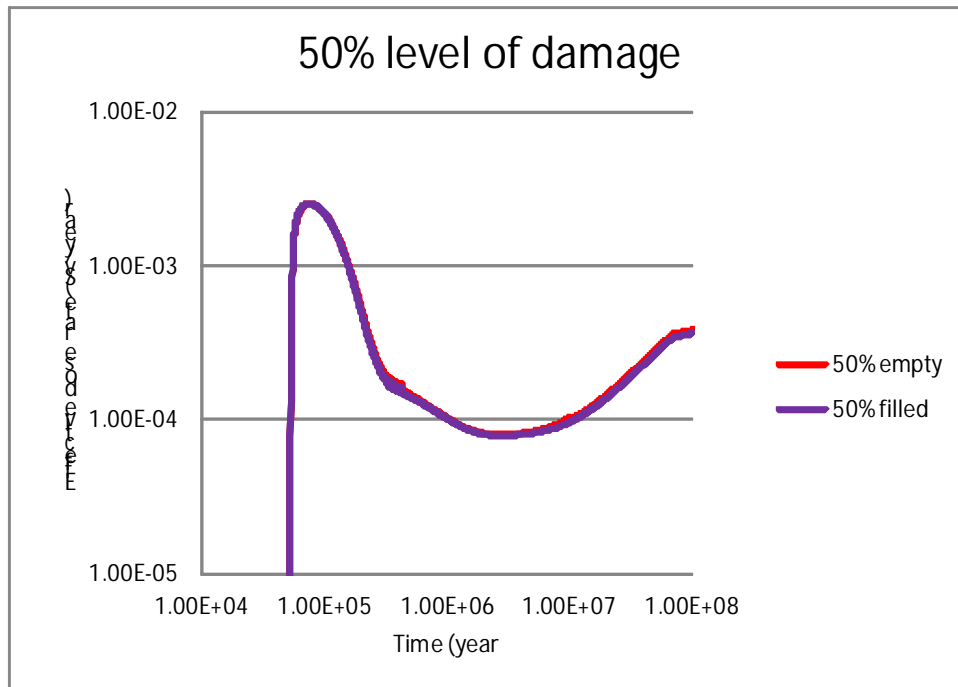


Fig. 48 Comparison of the development of the effective dose rate with concern to the empty and filled erosion channels with 50% damage to the bentonite layer.

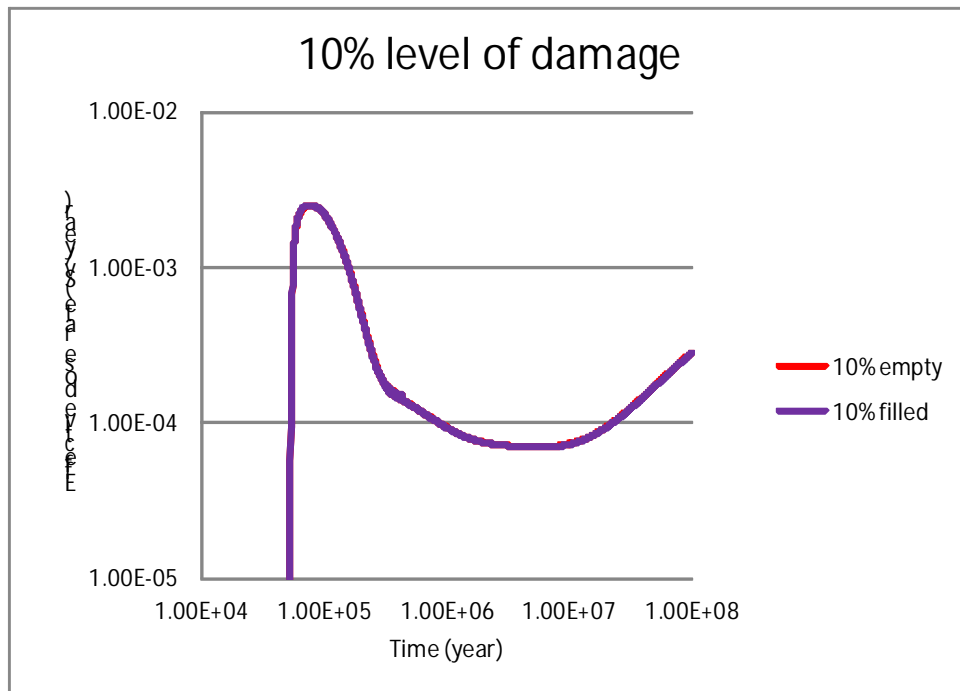


Fig. 49 Comparison of the development of the effective dose rate with concern to the empty and filled erosion channels with 10% damage to the bentonite layer.

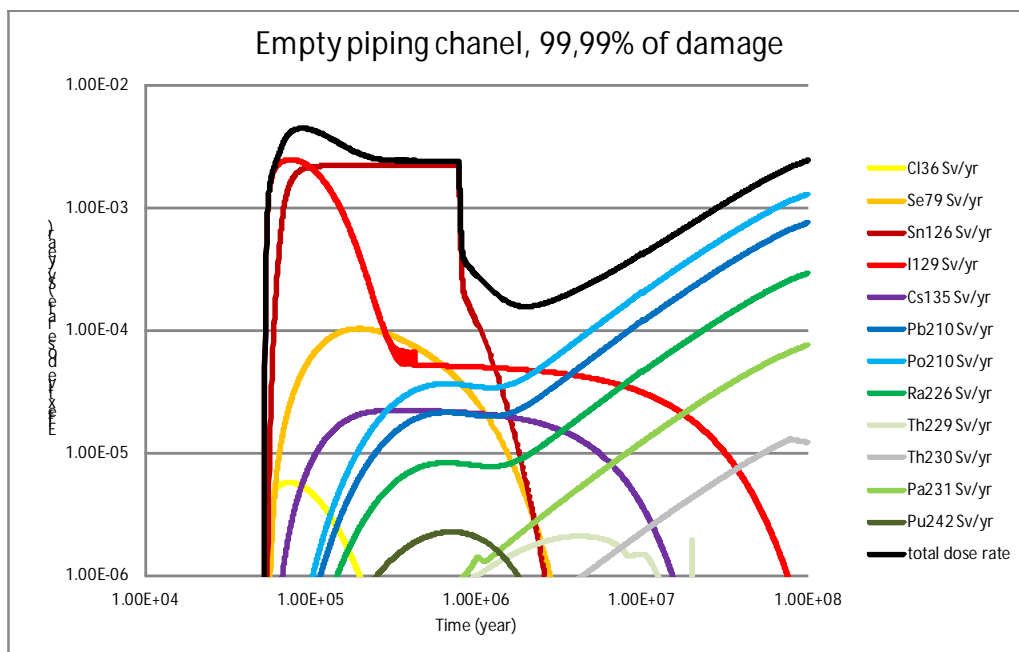


Fig. 50 The contributions of individual radionuclides to the total effective dose rate in the case of the empty erosion channel when simulating 99.99% damage to the bentonite layer.

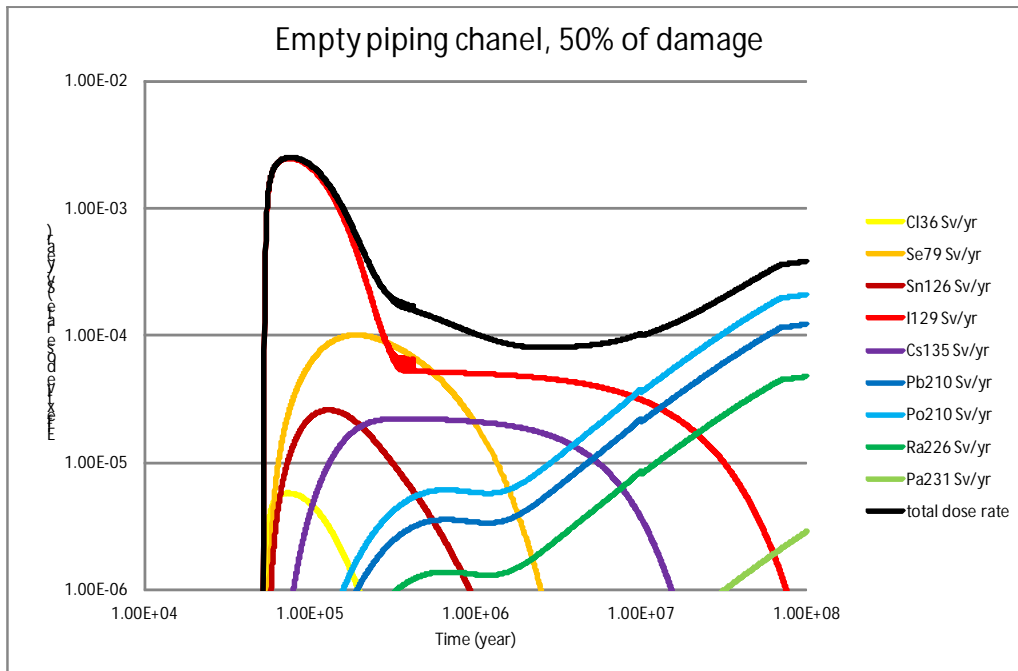


Fig. 51 The contributions of individual radionuclides to the total effective dose rate in the case of the empty erosion channel when simulating 50% damage to the bentonite layer.

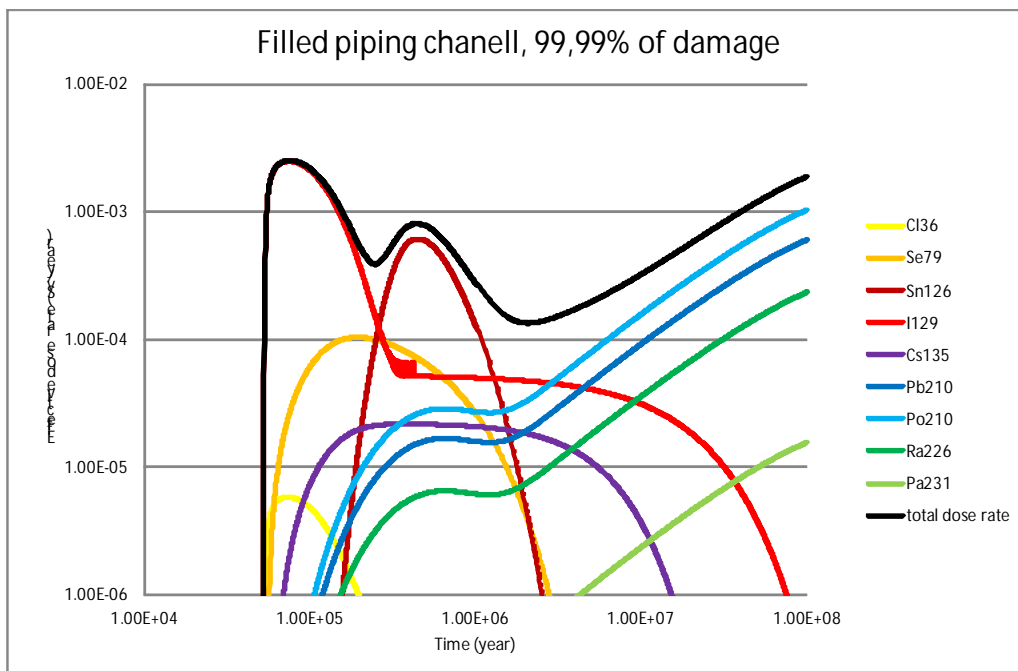


Fig. 52 The contributions of individual radionuclides to the total effective dose rate in the case of the filled erosion channel when simulating 99.99% damage to the bentonite layer

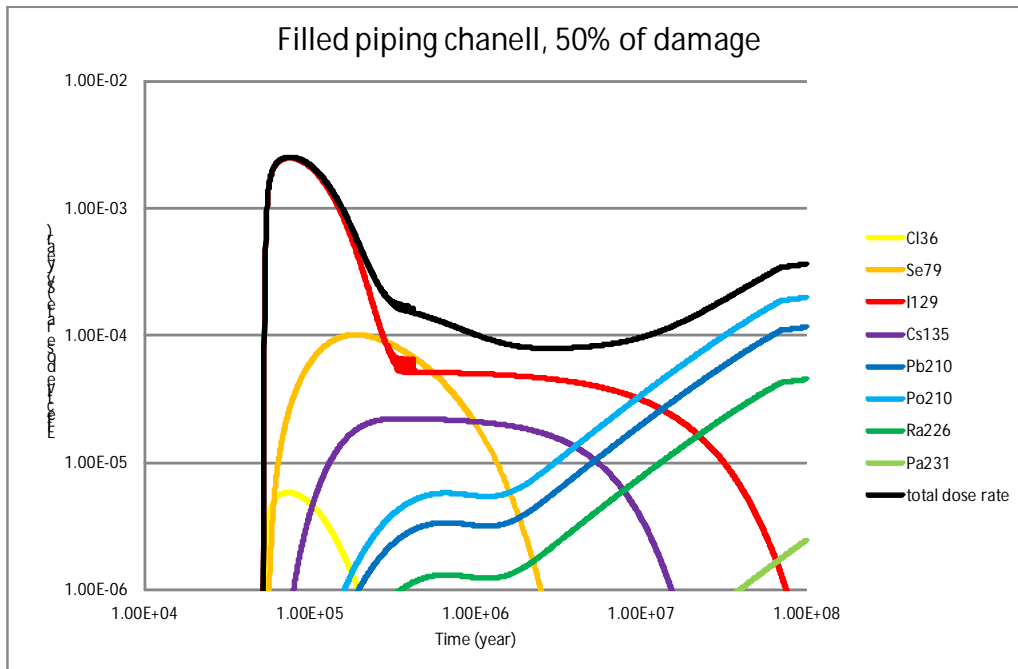


Fig. 53 The contributions of individual radionuclides to the total effective dose rate in the case of a filled erosion channel when simulating 50% damage to the bentonite layer.

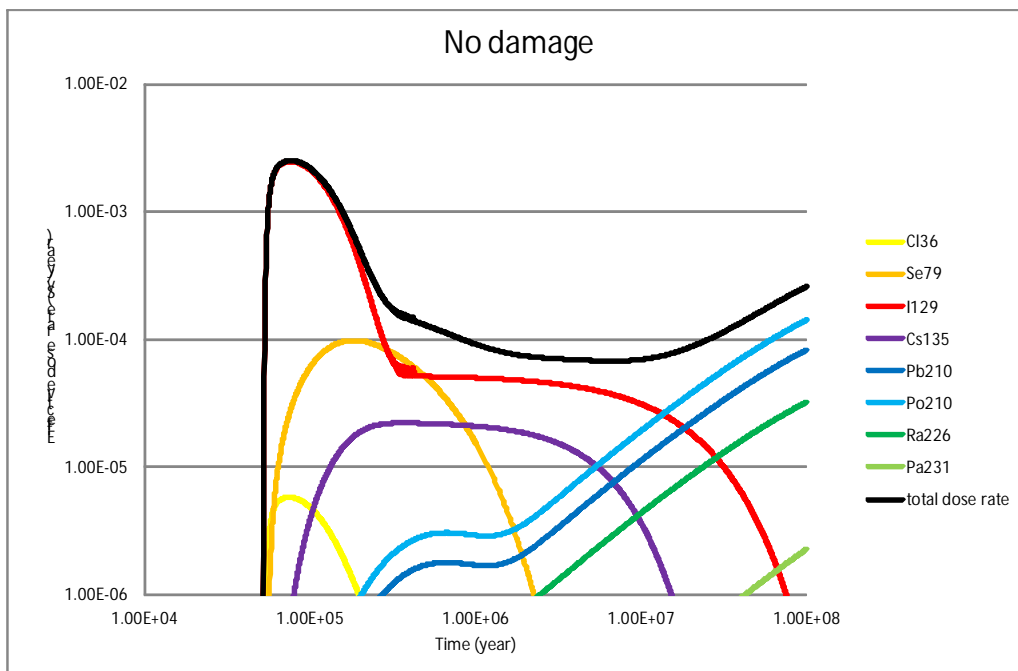


Fig. 54 The contributions of individual radionuclides to the total effective dose rate in the case of an intact bentonite layer

The results show that the state of the bentonite layer has a significant influence not only on the effective dose rate, but also on changes concerning the dominant critical radionuclides.



However, it should be noted that cases involving a larger erosion channel radius are completely unrealistic and served only for parametric study purposes; none of the scenarios covered in the deep geological repository development programme in the Czech Republic consider the washing out of the bentonite to the extent simulated herein.

## 7. Modelling of the EPSP experiment

### 7.1 Experiment description

The conceptual design of the EPSP includes the components shown in Figure 55:

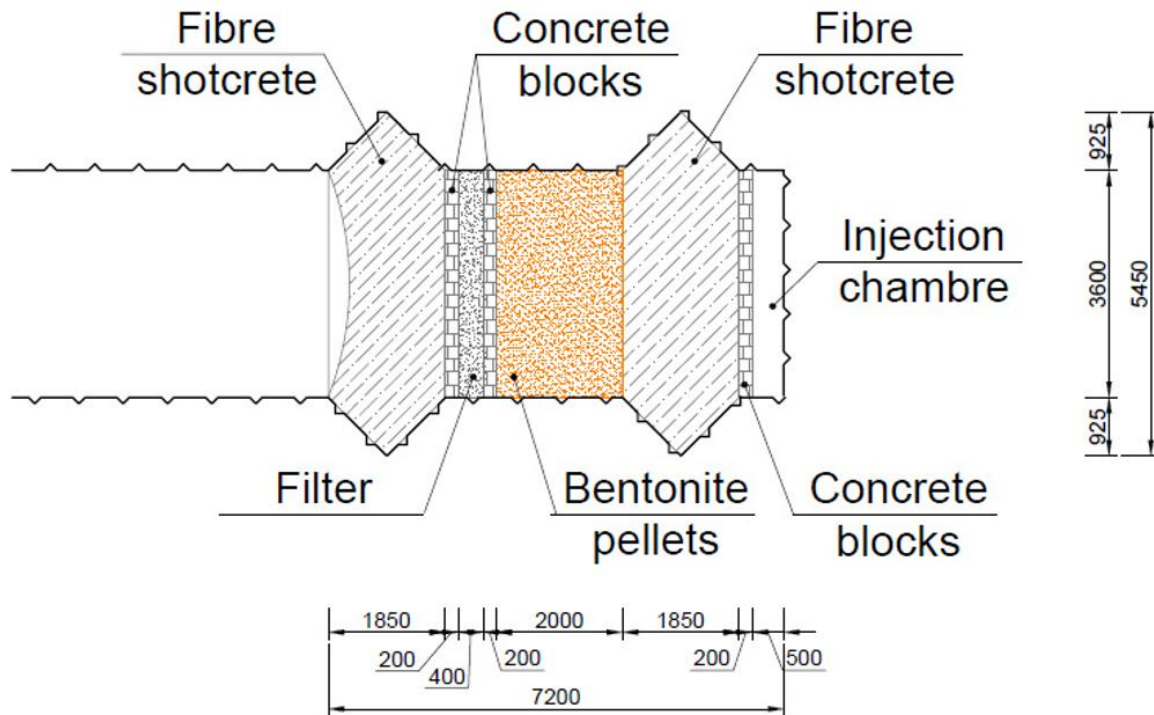


Fig. 55 EPSP design

**Pressure Chamber:** The pressure chamber consists of an open area that can be used to pressurise the inner concrete plug. The chamber contains an inlet valve and a drain valve that can be used to fill the chamber with air (gas), water or a bentonite slurry. The chamber was constructed to be as small as possible so as to allow the pressure to be more easily controlled. The pressure chamber is sealed with a special membrane.

**Concrete Walls:** Concrete walls were used in order to facilitate the construction of the EPSP. Three concrete walls were built: (i) a wall between the pressure chamber and the inner



concrete plug, (ii) a wall between the bentonite and the filter, and (iii) a wall between the filter and the outer concrete plug.

**Inner Concrete Plug:** The inner concrete plug makes up one of the sealing components of the EPSP and was constructed of sprayed fibre concrete. The fibre concrete has a relatively low pH value; the recipe and pH values were determined during the detailed design stage.

**Sprayed Bentonite Pellets:** The bentonite pellet zone comprises B75 bentonite - a natural, high-smectite content Ca-Mg bentonite with a notably high iron content in the octahedral layer of the smectite. The purpose of the bentonite is to seal and absorb/adsorb any water that leaks across the inner concrete plug. The bentonite zone is 2m long.

**Filter:** The filter collects any water that is not absorbed by the bentonite. This is most likely to occur if the leakage rate across the inner concrete plug is sufficient to allow for the piping and erosion of the bentonite to occur. The filter is also used to reverse the direction of pressurisation of the EPSP.

**Outer Concrete Wall:** The outer concrete plug is designed to keep the other components of EPSP in place. However, should the direction of pressurisation of the EPSP be reversed, the outer concrete plug will have to perform as well as the inner concrete plug and, therefore, the requirements concerning the outer concrete plug are the same as those concerning the inner concrete plug.

A series of pressure tests was carried out on the inner concrete plug before the bentonite was emplaced so as to test the quality of the plug and to decide, following inspection, whether grouting around the plug was required. This initial pressurisation was carried out using air and water. The tests confirmed that additional grouting was indeed required.

Following the emplacement of the bentonite, the second concrete plug was constructed. Subsequently, pressure tests were conducted which confirmed the need for additional grouting.

The EPSP plug was pressurised using water to a maximum of 1MPa whereupon the saturation process commenced within the bentonite pellet zone.

Additional pressurisation from the filter was required so as to create improved conditions for bentonite saturation. The average pressure level within the EPSP experiment in the initial stage was 0.1MPa. Within two months the pressure had increased to 0.5MPa and, subsequently, to 1MPa.

As the experiment progressed, pressurisation from the filter part was terminated and the pressure was gradually increased.

## **7.2 Methodology and model**

Numerical simulation was conducted using the CODE\_BRIGHT finite element code for the thermo-hydro-mechanical (THM) analysis of geological media. A short description of this software is provided above in the section on laboratory experiment modelling.

The creation of a fully realistic model of the EPSP experiment was not the purpose of this project. Due to the complexity of the experiment and the large number of uncertainties, the model was simplified significantly. It presents a part of the experiment under “ideal” conditions and covers the bentonite pellet saturation process only. For reasons of



simplification, it assumes no gravity and a constant temperature of 12°C throughout the experiment. In addition, the team decided not to include mechanical behaviour in the first version of the model since for certain materials no mechanical parameters are available. Moreover, this process would probably not have a significant influence on the results of the experiment.

### 7.3 Geometry

The model's geometry is 2D axisymmetric and has the same dimensions as the real experiment (see Figure 55). However, not all the elements of the EPSP experiment are included in the model. It consists of one inner shotcrete plug, the bentonite pellet zone and a surrounding rock zone (Figure 56). The generated unstructured mesh features 2846 nodes and 5324 triangle elements.

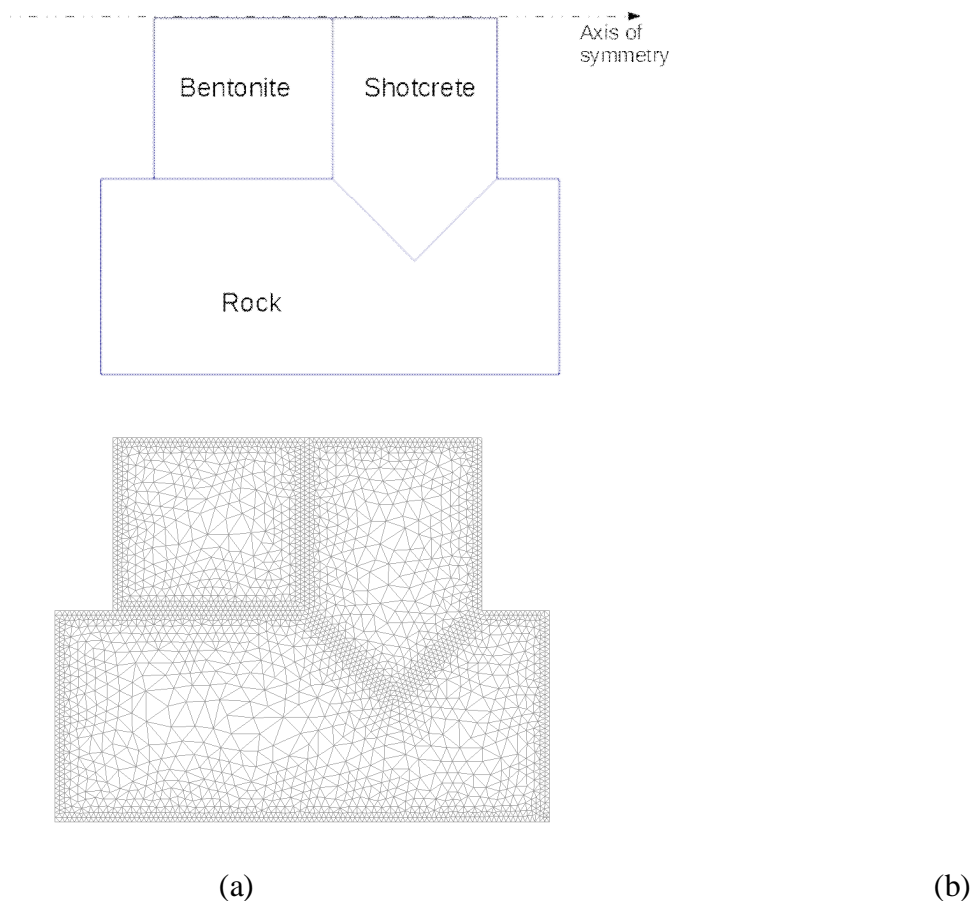


Fig. 56 Numerical model: (a) Geometry (b) Mesh

### 7.4 Material parameters

The mechanical and hydraulic parameters of the bentonite material were taken from the PHM model using bentonite pellets (see above).

Parameters regarding the retention curves of the shotcrete and rock materials were defined as being identical, see Table 12. The other parameters concerning these materials are presented in Table 13. During the course of the experiment, a high degree of local water flow was



observed. In all probability there were a number of fractures in the rock surrounding the experimental zone, so a relatively high (for such a type of rock) value of intrinsic permeability was employed.

Tab. 12 Parameters of the retention curves of the shotcrete and rock materials.

Parameters	ITYCL	P1	P2	P3	P4	P5
Retention curve	1	0.5	0.072	0.33	0	1

Tab.13 Parameters of the shotcrete and rock materials.

Material	Shotcrete	Rock
porosity	0.3	0.01
density	2600kg/m <sup>3</sup>	2860kg/m <sup>3</sup>
intrinsic permeability	1.e-15m <sup>2</sup>	1.e-13m <sup>2</sup>

## 7.5 Time intervals

The simulation process was divided into several time intervals which corresponded approximately to the different experimental stages:

- The first time interval (from 0 to 61 days) represents the initial hydration phase following the construction of the bentonite pellet zone. There was no additional pressure during this time; however, the bentonite began to draw water from the shotcrete plug and the host rock.
- The second time interval (from 61 to 82 days) represents a period of increasing pressure within the pressure chamber up to 0.2MPa, see Figure 57a.
- The third time interval (from 82 to 224 days) corresponds to pressurisation of 0.2MPa from both the pressure chamber and the filter, see Figure 57b.
- During the next time interval (from 224 to 264 days), the pressure was increased to 0.5MPa.
- During the final time interval (from 264 to 300 days), the pressure was increased to 1.2 MPa.

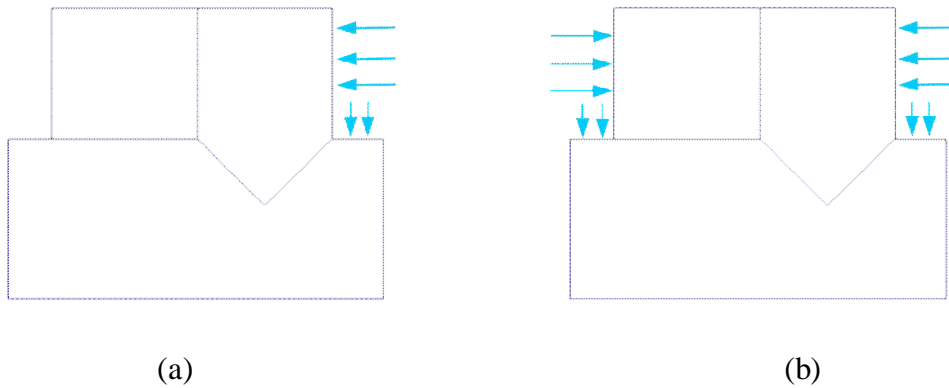
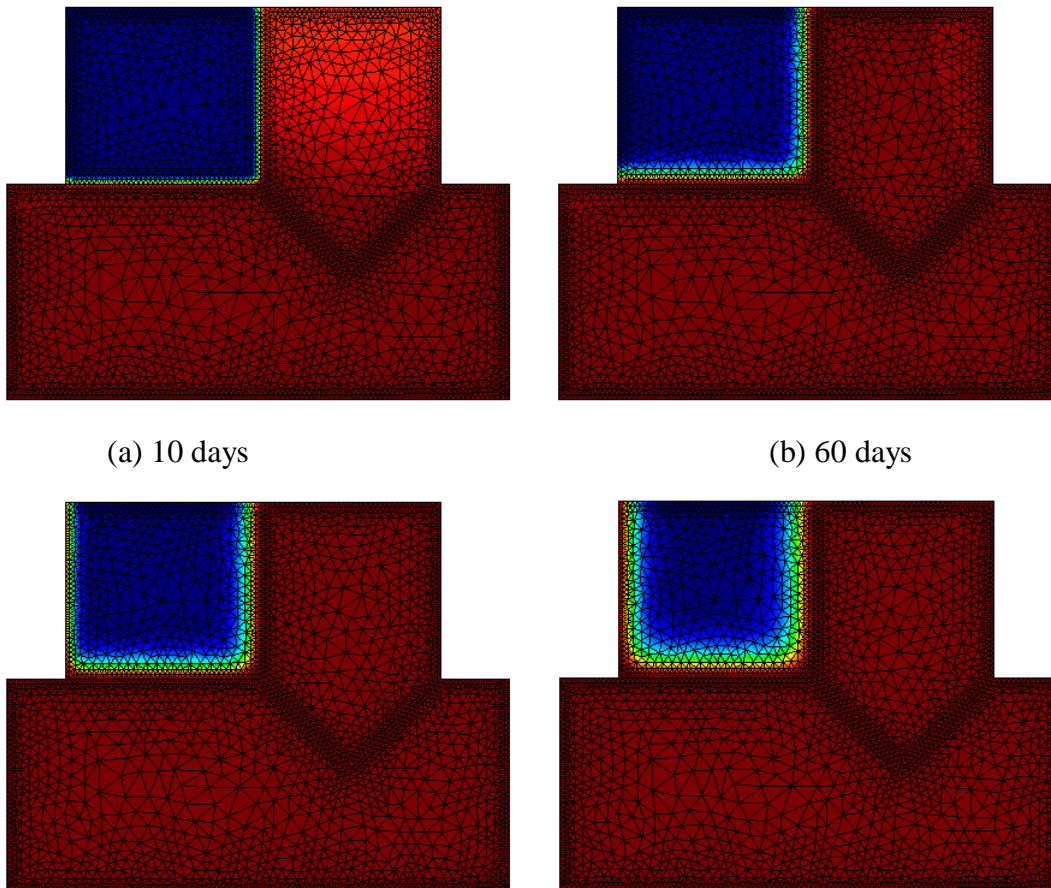


Fig.57 The pressurisation process

### 7.6 Modelling Results

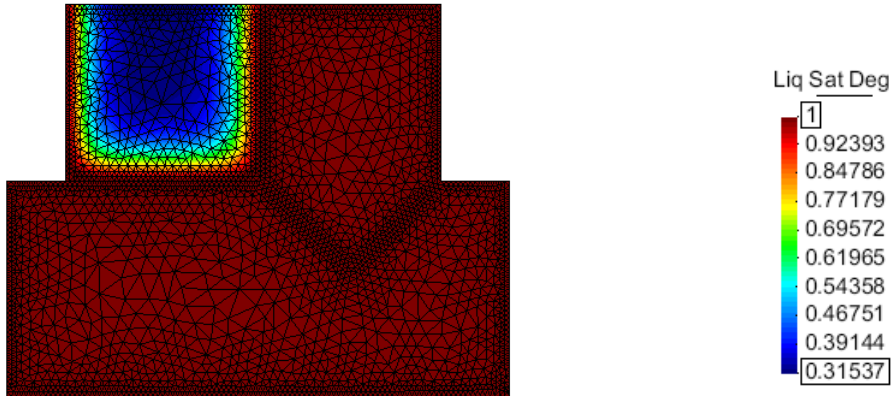
Figures 58 - 60 show the simulation of the bentonite saturation process over a total of 300 days. The saturation process occurs very slowly and a large part of the bentonite still exhibits a low level of saturation. It seems that increasing pressure from pressure chamber does not have a significant influence on the saturation process. That said, additional pressurization exerted from the gravel filter of the bentonite pellet zone appears to influence saturation substantially.





(c) 100 days

(d) 200 days



(e) 300 days

Fig.58 The saturation process

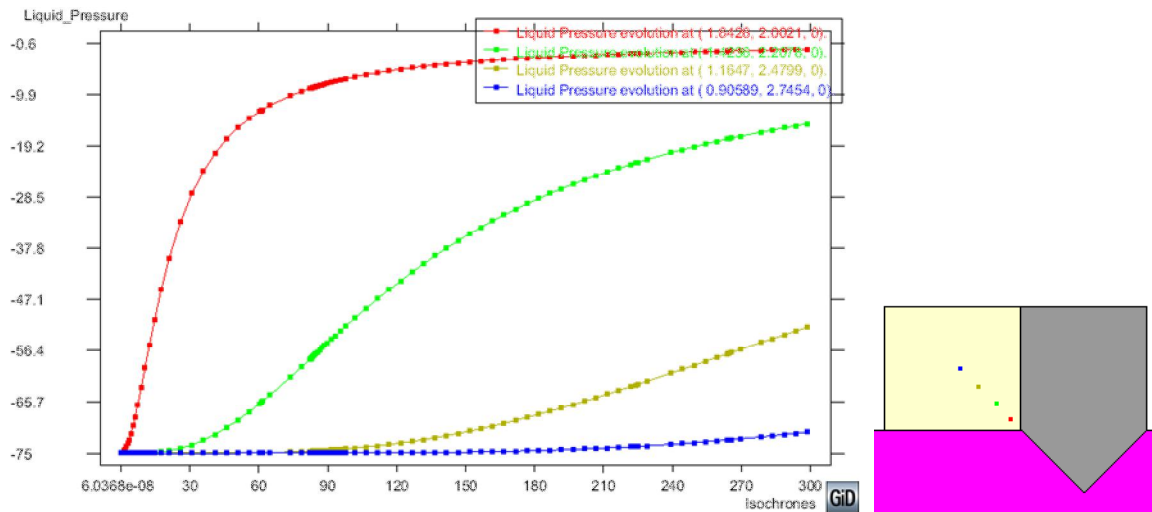


Fig. 59 The evolution of liquid pressure at different points within the bentonite zone.

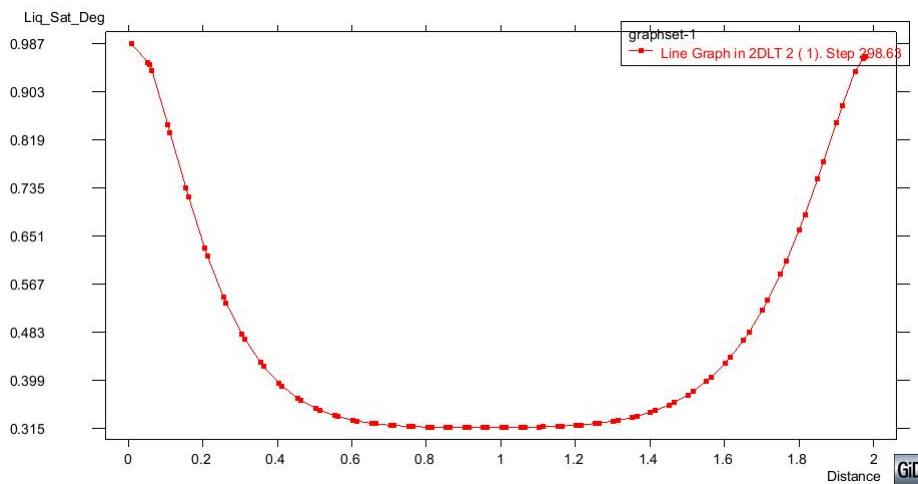


Fig. 60 Profile of bentonite saturation near the axis of symmetry after 300 days.

Figure 61 shows that the main part of the water flows out of the model through the rock. In all probability, increasing pressure only increases the outflow of water.

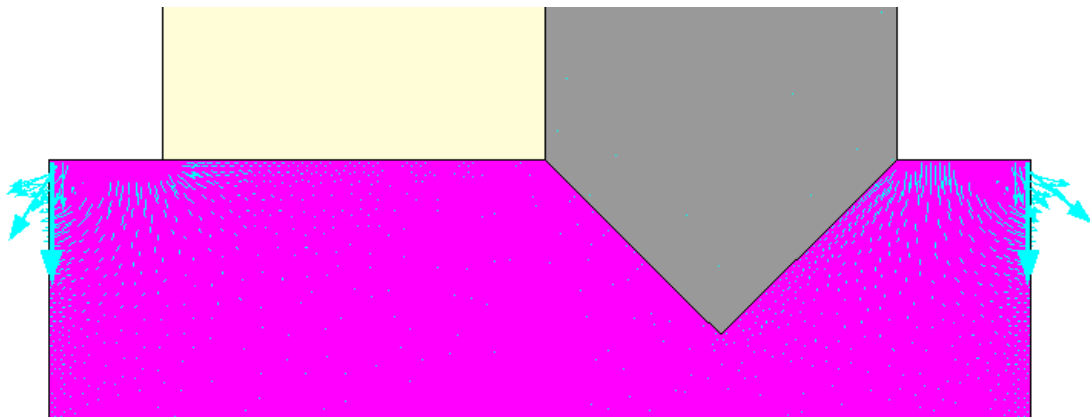


Fig.61 Liquid advection vectors, 300 days.

## 8. Conclusions

The model illustrates the saturation process within the bentonite pellet zone under “ideal” conditions. However, the numerical model of the EPSP experiment described herein is very simple and contains a large number of uncertainties and limitations. Currently, the results of the model correspond only weakly to the data gathered from the real physical experiment; however, the experiment remains ongoing and the research team plans to define a number of additional parameters which will contribute significantly towards improving the model.



## 9. Literature

Code\_bright tutorial manual. Universitat Polytechnica de Catalunya, Barcelona, 2014

[https://www.etcg.upc.edu/recerca/webs/code\\_bright/code\\_bright](https://www.etcg.upc.edu/recerca/webs/code_bright/code_bright) (19.8.2014).

Dvořáková, M., Hanusová, I., Svoboda, J., Vencel, M.: EPSP Experiment – Construction of a plug for a deep geological radioactive waste repository as part of the European DOPAS Project, Tunel 23, 2/2014.

GoldSim Contaminant Transport Module, User's Guide, Version 6.0, GoldSim Technology Group, Washington, USA, December 2010.

Landa, J., Trpkošová, D., Vetešník, A.: Tvorba celkového robustního modelu hodnocení bezpečnosti úložiště a aplikace modelu. Zpráva ÚJV 14276, ÚJV Řež, a. s., 2013.

Svoboda J.: testing plan for EPSP instrumentation and monitoring. Deliverable No. 3.18, CTU Prague, 2014.

Vašíček, R., Svoboda, J., Trpkošová, D., Večerník, P., Dvořáková, M.: Testing plan for the EPSP laboratory experiment. Deliverable No. 3.16, CTU Prague, 2013.

White, M., Doudou, S., Neall, F.: Design Bases and Criteria. Deliverable No. 2.1, Galson Sciences Limited, 2014.

Fiedler F., Oubram J., Erös J., Vozár J., Hamšík J., Prachař I., Blažek J. (2010): Aktualizace referenčního projektu hlubinného úložiště radioaktivních odpadů v hypotetické lokalitě. II. etapa - Varianty řešení a jejich návrh, F. Technologická část, ÚJV Řež a.s.

IAEA (2010): Handbook of parameter values for the prediction of radionuclide transfer in terrestrial and freshwater environments, Technical report no. 472, International Atomic Energy Agency, Vienna, 2010, [http://www-pub.iaea.org/MTCD/publications/PDF/trs472\\_web.pdf](http://www-pub.iaea.org/MTCD/publications/PDF/trs472_web.pdf)

Krásný J., Kněžek M., Šubová A., Daňková H., Matuška M., Hanzel V (1982): Odtok podzemní vody na území Československa, Český hydrometeorologický ústav, 1982

Landa J. (2012): Modelování vlivu vybraných parametrů migrace radionuklidů z úložišť radioaktivních odpadů na jejich přenos do biosféry. ČVUT v Praze, 2012.

Trpkošová D., Landa J., Chudoba J., Hokr M., Vetešník A., Vokál A. (2013): Výzkum a vývoj metodik hodnocení bezpečnosti úložiště. Zprava projektu FR-TI1/362, zpráva ÚJV 14020, červenec, 2013.

UPC – Universitat Plitecnica de Catalunya (2015): Code\_Bright Tutorial Manual. Barcelona, 327 p.

[https://www.etcg.upc.edu/recerca/webs/code\\_bright/downloads/tutorials/view](https://www.etcg.upc.edu/recerca/webs/code_bright/downloads/tutorials/view)

UPC – Universitat Plitecnica de Catalunya (2015a): Code\_Bright Users Guide. Barcelona, 183 p.

Villar, M. V., (2007): Water retention of two natural compacted bentonites. Clays and Clay Minerals, vol. 55, No. 3, 311-322.

[https://www.etcg.upc.edu/recerca/webs/code\\_bright/downloads/manual-users-guide-v4/view](https://www.etcg.upc.edu/recerca/webs/code_bright/downloads/manual-users-guide-v4/view)

Vokál A., Havlová V., Hercík M., Landa J., Lukin D., Vejsada J. (2010): III. etapa Studie zadávací bezpečnostní zprávy; C. Dokumentární část; C.2 Hodnocení bezpečnosti



Aktualizace referenčního projektu hlubinného úložiště radioaktivních odpadů v hypotetické lokalitě. Ústav jaderného výzkumu Řež a.s., 09/2010

**Online:**

BIMP: Bureau International des Poids et Mesures, Monographie BIPM-5  
<http://www.bipm.org/en/publications/monographie-ri-5.html>

NuDat 2.6: Interactive Chart of Nuclides, The National Nuclear Data Center, USA  
<http://www.nndc.bnl.gov/nudat2/>